Available online at www.sciencedirect.com

ScienceDirect

Geochimica et Cosmochimica Acta 284 (2020) 1–20

Geochimica et Cosmochimica Acta

www.elsevier.com/locate/gca

Mixing of carbonatitic into saline fluid during panda diamond formation

Fang Huang [a,b,*], Dimitri A. Sverjensky [b]

[a] CSIRO Mineral Resources, Kensington, WA 6151, Australia

[b] Department of Earth & Planetary Sciences, Johns Hopkins University, 3400 North Charles Street, Baltimore, MD 21218, USA

Received 7 January 2020; accepted in revised form 8 June 2020; available online 17 June 2020

Abstract

Diamonds containing fluid inclusions provide invaluable samples of upper mantle fluids, the study of which illuminates not only diamond formation but also the long-term evolution of the subcratonic, lithospheric mantle. The very large range of inclusion compositions worldwide has been interpreted to represent four end-member fluids: saline (rich in Na + K + Cl); silicic (rich in Si + Al); and carbonatitic (rich in Ca + Mg + Fe, with low-Mg and high-Mg end members). However, the sources and evolution of these fluids and the processes involved in diamond formation are still unclear.

We used an unusual study of diamonds from the Panda kimberlite (Ekati Mine, Northwest Territories, Canada) in which both mineral and fluid inclusions in the diamonds were analyzed (Tomlinson et al., 2006) to develop models of the saline, silicic, and low-Mg carbonatitic fluids present in the Panda fluid inclusions. The models used aqueous speciation and solubility calculations to link the solid and fluid inclusion chemistry with model upper mantle rock types. We used the extended Deep Earth Water model to calculate equilibrium constants previously calibrated with experimental rock solubilities referring to upper mantle temperatures and pressures (Huang and Sverjensky, 2019). Our results at 950 °C and 4.5 GPa suggest that the saline fluid could originate from peridotite, the silicic fluid from eclogite, and the low-Mg carbonatitic fluid from carbonated dunite.

The fluid models were then used to predict the irreversible, chemical mass transfer when the carbonatitic fluid infiltrated a harzburgite containing a saline fluid. Simultaneous reduction of formate and bicarbonate in the carbonatitic fluid and oxidation of aqueous hydrocarbons from the peridotitic fluid during mixing and reaction with harzburgite resulted in the formation of diamond, olivine, garnet, and clinopyroxene, and increases in the $logf_{O_2}$ and pH. Olivine was predicted to become more Fe-rich and garnet more Ca and Fe-rich with reaction progress, in agreement with reported temporal trends (core-to-rim) in the Panda mineral inclusions. The fluid at the site of diamond formation became more saline with reaction progress and the predicted aqueous phase concentrations of all elements changed consistent with trends in Panda fluid inclusions. In contrast, a prediction for a saline fluid infiltrating a harzburgite containing a carbonatitic fluid resulted in trends of the silicate minerals and the salinity with reaction progress that were in the opposite direction to data from the Panda diamonds. Overall, our study strongly supports the notion that fluids from subducting slabs could mix and precipitate diamonds containing carbon from both oxidized and reduced sources, while adding Ca and Fe to the sub-lithospheric cratonic mantle through metasomatic reactions.

© 2020 Elsevier Ltd. All rights reserved.

Keywords: Diamond; Vaccine manufacturing; Inclusions; DEW model; Thermodynamic modeling; Fluid mixing

* Corresponding author at: CSIRO Mineral Resources, Kensington, WA 6151, Australia.
E-mail address: f.huang@csiro.au (F. Huang).

https://doi.org/10.1016/j.gca.2020.06.011
0016-7037/© 2020 Elsevier Ltd. All rights reserved.

1. INTRODUCTION

Fluids in the deep Earth are thought to play an important part in the long-term geochemical cycling of elements through subduction-zones (Scambelluri and Philippot, 2001; Malaspina et al., 2010; Sanchez-Valle, 2013; Ague and Nicolescu, 2014; Manning, 2014; Mikhail and Sverjensky, 2014; Sverjensky et al., 2014a; Weiss et al., 2015; Galvez et al., 2016; Piccoli et al., 2016; Plümper et al., 2017; Vitale Brovarone et al., 2017; Connolly and Galvez, 2018; Barry et al., 2019), in mantle metasomatism and its influence on the re-fertilization and the tectonic stability of the subcratonic, lithospheric mantle (Menzies and Hawkesworth, 1986; Carlson et al., 2005; Pearson and Wittig, 2008; O'Reilly and Griffin, 2013; Miller et al., 2014; Wang et al., 2015; Weiss et al., 2016), and the formation of diamonds (Tomlinson et al., 2006; Stachel and Harris, 2008a; Shirey et al., 2013; Stachel and Luth, 2015; Sverjensky and Huang, 2015; Weiss et al., 2015; Bureau et al., 2018). Unlike the directly measurable compositions of xenocrysts and xenoliths brought up to the surface by magmas, direct evidence of natural fluid compositions can only be revealed in fluid inclusions. Due to the chemical stability of diamonds, fluid inclusions in diamonds offer the most robust evidence of deep Earth fluids, which makes diamonds so valuable scientifically (Navon, 1999; Klein-BenDavid et al., 2007; Weiss et al., 2009; Weiss et al., 2014; Jablon and Navon, 2016).

Diamonds also often preserve solid inclusions of silicates and other minerals that may reflect the conditions of diamond formation in the deep Earth (Stachel and Harris, 2008a; Walter et al., 2011). Evidence from solid and fluid inclusions in diamonds forms a complementary set of information to measurements on xenoliths and xenocrysts, which may be affected by alteration processes during uplift. Most studies of mineral inclusions in diamonds broadly assume that the chemical and isotopic compositions of the inclusions are representative of the co-formation of the inclusions and the host diamonds, i.e. they are syngenetic. Experimental studies of diamond synthesis from complex fluids and melts show that syngenetic mineral inclusions form readily in synthetic diamonds (Bureau et al., 2016, 2018). However, it has also been suggested that at least some mineral inclusions in monocrystalline diamonds represent fragments of the pre-existing upper mantle (Taylor et al., 2016; Nestola et al., 2017), i.e. they are protogenetic. In such cases, the very low H contents of silicate inclusions such as olivine may not record the passage of metasomatic fluids.

In several studies it has been possible to obtain microprobe compositions of solid inclusions in the monocrystalline cores and fibrous rims of the same diamonds from the Kaapvaal Craton, South Africa (Izraeli et al., 2004) and from the Superior and Slave Cratons, Canada (Tomlinson et al., 2006; Miller et al., 2014). In these cases, the mineral inclusions in the fibrous diamonds appear to record a metasomatic alteration of the inclusions in the monocrystalline diamonds. Specifically, inclusions of olivine and garnet in fibrous diamonds show distinctive trends extending from the compositions of the inclusions in monocrystalline diamonds towards enrichment in Ca and Fe, and towards the compositions of the carbonatitic fluids in the fluid inclusions in the fibrous diamonds (Weiss et al., 2015). These trends strongly suggest that the metasomatic fluids involved in the formation of these particular diamonds have strongly influenced the chemistry of the olivine and garnet inclusions, regardless of their ultimate origin. It is interesting to note that the trends towards Ca and Fe enrichment in such mineral inclusions are consistent with trends in metasomatic re-fertilization of upper mantle rocks (Miller et al., 2014).

The major, trace element, and isotopic compositions of fluid inclusions in diamonds have also been extremely useful in delineating different groups of diamonds, suggesting different sources of the carbon, and inferring fluid mixing or reaction processes during diamond formation (Schrauder et al., 1996; Izraeli et al., 2001; Shiryaev et al., 2005; Tomlinson et al., 2006; Klein-BenDavid et al., 2007; Weiss et al., 2009; Klein-BenDavid et al., 2010; Weiss et al., 2013; Klein-BenDavid et al., 2014; Frezzotti, 2019; Sobolev et al., 2019). The averaged compositions of major elements (Na, K, Si, Al, Ca, Fe and Mg) of fluid inclusions in diamonds worldwide vary widely and define four end member compositions: 1) a saline end member rich in K, Na, and Cl; 2) a silicic end member rich in Si with much less Al; 3) a low Mg-carbonatitic end member, low in Mg relative to Ca and Fe, and low in Al and Si; 4) a high Mg-carbonatitic fluid, high in Mg relative to Ca and Fe, and again low in Al and Si (Izraeli et al., 2001; Shiryaev et al., 2005; Tomlinson et al., 2006; Klein-BenDavid et al., 2007; Weiss et al., 2009; Weiss et al., 2015). The term carbonatitic end-member has that name partly because it has been assumed that the main anion balancing the Ca, Mg, and Fe cations in the fluid is carbonate or that these inclusion fluids may represent a water-bearing carbonatitic melt (Weiss et al., 2015).

Representative fluid inclusion compositions from diamonds worldwide are plotted in Fig. 1a and b (also see Appendix A) and from the Panda diamonds (Tomlinson et al., 2006) in Fig. 1c and d. It should be noted that in plots such as Fig. 1a and c, the low- and high-Mg carbonatitic fluids are not distinguishable. However, they are distinguishable in Fig. 1b and d. The high-Mg carbonatitic fluids are not recorded in the Panda diamonds, so we focus here on the saline, the silicic, and the low-Mg carbonatitic end-member fluids. It can be seen in Fig. 1a that although the worldwide inclusion fluids vary over wide ranges of composition, the three end members are well separated by the ends of two linear arrays. However, the intermediate fluid compositions between the silicic and saline end members are very uncommon (Weiss et al., 2009; Weiss et al., 2015). The three end members shown in Fig. 1a suggest that different fluid sources and evolution histories may apply during diamond formation worldwide. Usually inclusions in any particular diamond lie on just one of the two arrays. Only inclusions in a single diamond from the Diavik kimberlite lie on two of the arrays (Klein-BenDavid et al., 2004).

In the present study, we focus on diamonds from the Panda kimberlite because of the unique set of data obtained

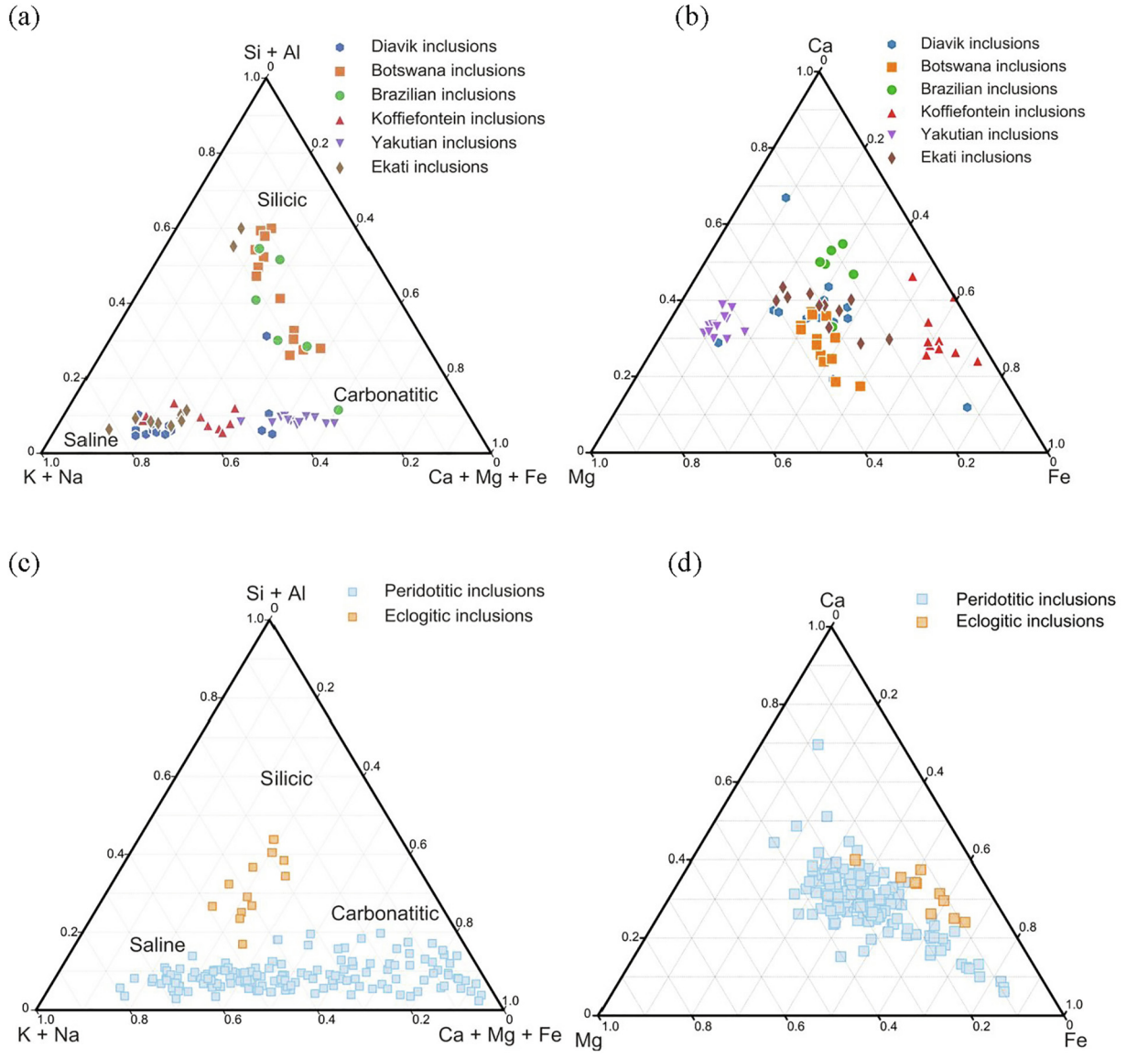

Fig. 1. Grouped major element compositions of fluid inclusions expressed as atomic, molar proportions: (a) and (b) Global diamonds; (c) and (d) Panda diamonds. Each data point in (a) and (b) represents an average composition of individual diamonds, whereas in (c) and (d) measurements of individual inclusions are depicted. Data source references are listed in Appendix A.

from the analysis of both the solid and aqueous fluid inclusions in individual Panda diamonds (Klein-BenDavid et al., 2007; Weiss et al., 2009; Shirey et al., 2013). Furthermore, comparisons of the compositions of solid inclusions in the fibrous rims with those in monocrystalline diamonds from the Panda kimberlite yielded evidence of metasomatic activity by fluids during diamond formation (Tomlinson et al., 2006). We investigated the application of equilibrium and irreversible, mass transfer, fluid-rock interaction models in order to establish how many of the observed characteristics of diamond fluid/solid inclusions and diamond formation could be explained without consideration of melts. By doing this, we do not mean to indicate that melts are not important in some aspects of diamond formation. Indeed, the temperatures and pressures relevant to at least some diamond formation are such that there can be a physical and chemical continuum between aqueous fluids and melts, although much disagreement exists between the exact conditions under which miscibility occurs (Dvir and Kessel, 2017). The temperature and pressure range of the Panda diamonds, however, refers to sub-solidus conditions in rocks of harzburgitic composition (Tomlinson et al., 2006; Stachel and Harris, 2008b). Stachel and Luth (2015) have suggested that diamond formation in the harzburgitic environment typically involves sub-solidus, fluid metasomatism without a significant role for melts.

The fluid inclusion compositions recorded in the Panda diamonds (Fig. 1c) mainly define a linear array between saline and carbonatitic end-member fluids. A second, less well-defined array of points (from only one diamond) extends

towards a silicic end-member fluid (see correlations with chloride in Appendix B). We have previously identified the silicic end member as a fluid in equilibrium with a coesite-bearing eclogite, which gives very high concentrations of silica relative to other inorganic solutes, in agreement with the fluid inclusion data (Sverjensky and Huang, 2015). This result enabled a study of the formation of diamond in a generic model eclogitic environment corresponding to the carbonatitic to silicic array of fluid compositions in Fig. 1a (Sverjensky and Huang, 2015).

Most diamonds worldwide are reported to have formed in peridotitic environments involving the saline fluid end member. Consequently, the present study is focused on explaining the saline-carbonatitic array for the Panda diamonds in Fig. 1c, as well as the distinctive compositional trends involving Ca and Fe enrichment in solid inclusions in the Panda diamonds. These features cannot be adequately explained using a traditional C-O-H fluid model (Duan and Zhang, 2006; Zhang and Duan, 2009) because the C-O-H model does not contain any of the chemical elements depicted in Fig. 1. In turn, this prevents a comprehensive model of diamond formation in realistic upper mantle environments. In the present study, we seek to go beyond the traditional notion that the carbon species during diamond formation in the deep Earth are composed of simple mixtures of volatiles such as H_2O, CO_2, CH_4, and H_2 (Stachel and Luth, 2015).

We have built a new version of the Deep Earth Water (DEW) model (Huang and Sverjensky, 2019) calibrated with the solubilities of eclogite and peridotite under upper mantle conditions (Kessel et al., 2005; Dvir et al., 2011; Kessel et al., 2015) to enable the calculation of equilibrium constants consistent with experimentally measured solubilities. It should be noted that the experimental rock solubilities used for the calibration of the DEW model extend from 700 to 1,000 °C and from 4.0 to 5.0 GPa, which covers the modeling regime of the present study. The details of this calibration are reported in Huang and Sverjensky (2019). A detailed summary of the basis of the equations of state used for the aqueous species is given in Sverjensky (2019). Our calibration included provision for the variable activity of H_2O and aqueous activity model for neutral dissolved gases such as CO_2 so that geologically reasonable chemical mass transfer calculations could be carried out.

Our recent theoretical (Sverjensky et al., 2014b) and experimental diamond anvil cell studies (Huang et al., 2017), together with other experimental (Li, 2017; Tumiati et al., 2017) and field and laboratory studies (Brovarone et al., 2017; Frezzotti, 2019; Sobolev et al., 2019) suggest that organic carbon species such as aqueous aliphatic acid anions, and even fluid hydrocarbons, may be of importance under upper mantle conditions (Sverjensky et al., 2020). Consequently, we have also taken into consideration the possible importance of aqueous metal–organic complexes at elevated temperatures and pressures. By incorporating all these calculated equilibrium constants into the data files for aqueous speciation, solubility, and chemical mass-transfer codes, it becomes possible to model the full spectrum of diamond fluid inclusion and solid inclusion compositions during the fluid-rock interactions involved in diamond formation.

2. GEOLOGIC SETTING OF THE PANDA KIMBERLITE AND THE NATURE OF THE UPPER MANTLE BELOW IT

The Panda kimberlite erupted into the Archean Slave Craton, Northwest Territories, Canada. The kimberlite eruption age is dated to be 53.3 ± 0.6 Ma using a Rb-Sr isochron based on phlogopites (Creaser et al., 2004). Numerous studies have indicated that the mantle below the Slave Craton has an unusual structure and distribution of major rock types compared with other well-studied cratons. The mantle lithosphere below the Slave craton has a two-layer structure: the top layer mainly consists of harzburgite and is described as a highly depleted layer, i.e. olivine-rich; but the bottom layer is dominated by lherzolite (Griffin et al., 1999). The boundary between the two layers is located at a depth of ~150 km, meaning that diamond formation is in principal possible from the bottom of the top layer all the way to the bottom layer (Griffin et al., 1999; Tomlinson et al., 2006). This two-layer lithospheric structure is unique among worldwide Archean mantle lithospheres (Griffin et al., 1999).

The formation pressures and temperatures of the Panda diamonds provided in Tomlinson et al. (2006) were calculated as follows: the pressures were based on the Cr-clinopyroxene geobarometer (Nimis and Taylor, 2000) applied to inclusions in the PAN3 and PAN5 coated diamond samples; the temperatures were estimated based on geothermometry of non-touching garnet-olivine and garnet-pyroxene pairs (Krogh, 1988; Nimis and Taylor, 2000) in the PAN3, PAN5 and PAN8 diamonds. The calculated temperature–pressure conditions for formation of the coated Panda diamonds are from 930 to 1,010 °C, and 4.2 to 4.6 GPa (Tomlinson et al., 2006). These ranges are sufficiently narrow that for our model calculations we chose a single set of representative conditions at 950 °C and 4.5 GPa. It should be noted that this temperature and pressure are at the low end of many other estimated conditions of diamond formation (Stachel and Luth, 2015).

Tomlinson et al. (2006) was not able to measure or calculate the oxygen fugacity of their Panda samples. However, measurements of the oxygen fugacity of peridotite xenoliths from the Diavik diamond mine in the same province as the Panda kimberlite showed a wide range of $logf_{O_2}$ values relative to the quartz-fayalite-magnetite (QFM) buffer from QFM + 1.0 to QFM − 3.8 (Creighton et al., 2010). Samples from the ultra-depleted layer (at less than 140 km depth) were the most oxidized (QFM + 1.0 to −0.6), and samples from depths greater than about 140 km were more reduced (QFM −1.0 to −3.8). Revaluation of the compositional data for these xenoliths using revised thermodynamic data has resulted in a slightly different range $logf_{O_2}$ values from QFM + 0.03 to QFM −3.73 (Miller et al., 2016). Our aqueous speciation models of the fluid inclusion data (discussed below) include independently derived values of $logf_{O_2}$ for the three end-member fluids represented in the Panda fluid inclusions.

3. METHODS

We first analyzed the fluid inclusion data from Tomlinson et al. (2006) to establish the compositions of the end-member fluids for the Panda diamonds. The end-member compositions were retrieved by linear extrapolation of the data as a function of chloride concentration as described below. Second, in order to build aqueous speciation and solubility models of the end-member saline, siliceous, and carbonatitic fluids we used mineral compositions based on the measurements of the solid inclusions in the Panda diamonds. For reasons discussed below, we choose to use mineral assemblages representative of harzburgite, eclogite, and carbonated dunite lithologies to model the saline, silicic, and carbonatitic end-member fluids, respectively. The specific mineral compositions were used as input to the aqueous speciation and solubility model (EQ3) to fit the fluid inclusion end-member compositions as closely as possible.

Aqueous speciation and solubility models depend very heavily on the equilibrium constants and activity models for the aqueous species used in the models. In Huang and Sverjensky (2019) we have described our extension of the DEW model based on a theoretical analysis of the solubilities of synthetic peridotites and eclogites (Kessel et al., 2005; Dvir et al., 2011; Kessel et al., 2015). These efforts resulted in a quantification of new complexes involving, Mg, Fe, Ca, Al, Si, and C. The equilibrium constants for these species were calibrated with these experimental data or extrapolated using the DEW model were calculated at 950 °C and 4.5 GPa and incorporated into the data files for the aqueous speciation and solubility code (EQ3) and the chemical mass transfer code (EQ6). With the exception of two Fe-complexes, noted below in Section 3.2, all the other equilibrium constants were directly from the calibration study by Huang and Sverjensky (2019). As in the latter study, our aqueous speciation model also included a model for the variable activity of water and the activity coefficients of aqueous, neutral dissolved gases such as H_2CO_3, CO_2, CH_4, CO, and C_2H_6 as functions of the solute content of the fluid. These changes constitute a first step towards modeling fluids with high solute contents. Because the model activity coefficients for the neutral dissolved gas species are much greater than unity in the hypothetical 1.0 molal standard state, much less CO_2 is predicted relative to HCO_3^-, and H_2CO_3 is the most abundant oxidized C-species in the model, consistent with *ab initio* calculations (Pan and Galli, 2016). This aspect of the DEW model contrasts with the much higher relative concentrations of neutral dissolved gas species previously published (Sverjensky et al., 2014c; Sverjensky and Huang, 2015) in which the aqueous speciation calculations assumed unit activity coefficients for neutral dissolved gas species.

3.1. Compositions of fluid inclusion end members

Electron microprobe analyses (EMPA) of fluid inclusions in the coated Panda diamonds from Tomlinson et al. (2006) in Fig. 1c and d clearly show a much greater scatter of the data points compared with those in Fig. 1a and b. This is a consequence of the fact that Fig. 1a and b contain averaged values of multiple individual analyses. In contrast, in Fig. 1c and d individual measurements of inclusions are plotted, revealing the substantial uncertainties in analyzing very small inclusions. For example, the data points in the bottom right-hand corner of Fig. 1c approaching extremely high Ca + Mg + Fe values may indicate uncertainties in the individual analyses or possibly a mixture of aqueous fluids and carbonate melts.

Linear correlations of each element with Cl enabled a choice of end-member fluid compositions (Appendix B). Because the saline end-member fluid is enriched in Na + K and Cl, the high Cl-end of the fluid inclusion trend was taken to define the saline fluid end member. The silicic and carbonatitic end member-fluids are both low in Na + K. Consequently, the silicic and the carbonatitic end members were identified by the low Cl end of the fluid inclusion arrays in eclogitic and peridotitic diamonds, respectively. After applying linear regression methods to the data using the KaleidaGraph™ software, we chose Cl = 55 (mol%) to determine the chemical composition of the saline end-member fluid (Appendix B), and Cl = 10 (mol%) for both silicic (Appendix B) and carbonatitic end-member fluids (Appendix B). These end-member Cl values were chosen because Cl numbers (mol%) higher than 55 or lower than 10 resulted in extremely low or even negative amounts of other major elements. We calculated the relative concentrations of Na, K, Si, Al, Ca, Mg, Fe and Ba using this method. However, because there is no Ba mineral reported in the solid inclusions, we focused on the major elements, leaving Ba and other trace elements for a future study.

In order to obtain absolute molal concentrations of the elements in the fluid inclusion end members, it would be necessary to have a measurement of the amount of water in the fluid inclusions relative to the amounts of solutes. Estimations of the amount of water have been indirectly derived from infrared measurements of the water-CO_2 ratio in diamond fluid inclusions (Tomlinson et al., 2006). Using this ratio requires an estimate of the amount of carbon in the fluid. It has often been assumed that the latter can be estimated from the amount of carbonate ions required to charge balance the aqueous cations measured (Klein-BenDavid et al., 2009). However, after chloride, carbonate is probably not the only anion present. Organic anions and hydroxyl may play an important role. Consequently, we chose to use different methods to obtain the absolute molalities of the elements in the fluid inclusions. Because K is predicted to have a very simple aqueous speciation under these conditions, i.e. aqueous $K^+ \gg KCl^0 \gg K(OH)^0$, theoretical predictions of the total dissolved K based on the solubility of a K-rich mineral should be relatively insensitive to other elements in the model of fluid speciation. Therefore, for the saline fluid we used a predicted phlogopite solubility to obtain an estimate of the K-concentration that we could use to set the molalities of all the other elements, based on the relative proportions of each element to K derived above from the fluid inclusion measurements. For the silicic

and the carbonatitic fluids, the absolute K-concentration was treated as a fit parameter to aid fitting the concentrations of all the other elements. The results for the three end-member fluids are given in Table 1.

3.2. Mineral assemblages and compositions used to model the end-member fluids

3.2.1. Panda peridotitic fluid model

The peridotitic mineral assemblage used to set equilibrium with the fluids corresponds to a harzburgite containing olivine ($Fo_{92}Fa_{08}$), orthopyroxene ($En_{96}Fs_{04}$), garnet ($Prp_{80}Alm_{10}Grs_{10}$), phlogopite, and diamond, where Fo, Fa, En, Fs, Pyp, Alm, and Grs represent the components forsterite, fayalite, enstatite, ferrosilite, pyrope, almandine, and grossular, respectively (Whitney and Evans, 2010). The mole fractions of the components listed were taken from an averaged value of mineral inclusions in peridotitic diamonds (Tomlinson et al., 2006), with slight adjustments in order to achieve equilibrium of all the mineral components with the aqueous fluid. These mineral components were used to constrain the fluid speciation and solubility model (Table 2) assuming ideal site-mixing.

It should be noted that we assumed the peridotitic fluid to be in equilibrium with phlogopite even though no phlogopite was observed by Tomlinson et al. (2006) as an inclusion in diamond. As noted above, this assumption gives an upper limit for the K content of the fluid. In addition, we used the Na and Cl concentrations measured in the fluid inclusion analysis, owing to a lack of stable corresponding minerals containing any significant amounts of Na or Cl. Another assumption in the model involved one of the metal Cl-complexes. The equilibrium constants of the metal-chloride complexes were not constrained by experimental studies by Kessel et al. because all those experiments to date have involved Cl-free systems. At the very high chloride content of the saline fluid we found that our predicted logK (log equilibrium constant) for the $FeCl_2$ complex was too strong. At 950 °C and 4.5 GPa, the logK value had to be weakened by 1.0 units. It should be noted that this adjustment was also carried over for the other two end-member fluid models. All the other metal-chloride complexes we used were independently predicted in the DEW model. Finally, we obtained the $logf_{O_2}$ of the system by regression to refine the best fit to the fluid inclusion data. The *pH* of the fluid was calculated in the aqueous speciation model through charge balance taking into account all aqueous species in the model.

Table 1
Compositions (molal) of the three end-member fluids involved in Panda diamond formation established by extrapolation of trends in the fluid inclusion compositions of Panda diamonds carried out in the present study using data from Tomlinson et al. (2006). See Appendix B.

	Peridotitic	Eclogitic	Carbonatitic
Si	0.59	2.95	0.86
Al	0.10	0.18	0.18
Fe	0.87	0.87	3.56
Mg	0.51	0.46	2.16
Ca	0.63	0.98	2.20
Na	1.80	0.40	0.45
K	4.23	0.70	0.50
Cl	11.94	0.84	1.18

3.2.2. Panda eclogitic fluid model

In one Panda diamond, Tomlinson et al. (2006) found an omphacitic clinopyroxene inclusion, from which it was inferred that the diamond had formed in an eclogitic environment. This inference is supported by the fluid inclusion analyses from this diamond (Fig. 1c), which form a separate trend to all the other inclusion fluids from the Panda diamonds. In order to construct an eclogitic fluid model, we assumed a mineral assemblage consisting of clinopyroxene ($Di_{67}Hd_{26}Jd_{07}$), garnet ($Prp_{32}Alm_{50}Grs_{18}$), coesite, and diamond, where Di, Hd, and Jd represent diopside, hedenbergite, and jadite, respectively (Whitney and Evans, 2010). The composition of the clinopyroxene came from an analysis of the PAN4 diamond (Tomlinson et al., 2006), with slight adjustments to ensure equilibrium of all mineral components with the fluid. The garnet composition was calculated from an average composition for eclogitic diamonds in Stachel and Harris (2008b). We assumed that the fluid was in equilibrium with coesite in order to calculate a maximum silica concentration (Table 2). The mineral components were used to constrain the fluid speciation and solubility model, again assuming ideal site-mixing. In addition, we used the measured K and Cl concentrations from the fluid inclusions owing to a lack of minerals containing any significant amounts of K or Cl. As described above, we obtained the $logf_{O_2}$ by regression and the *pH* of the fluid was calculated as part of the aqueous speciation model through charge balance.

3.2.3. Panda carbonated dunitic fluid model

The origin of the carbonatitic end-member fluid inclusion composition is more enigmatic than that of the peridotitic or the eclogitic end members. Many authors (Klein-BenDavid et al., 2007; Weiss et al., 2011; Shirey et al., 2013) assumed that the carbonatitic end-member fluid is actually a hydrous carbonate melt. However, the question could be asked as to whether the observed characteristics of diamond formation involving carbonatitic fluids can be reproduced by models involving aqueous fluids instead of melts. If we assume that Panda diamonds formed in a harzburgitic sub-solidus environment (Stachel and Luth, 2015), then we can investigate the consequences of representing the carbonatitic end member as an aqueous fluid. A defining feature of carbonatitic fluid inclusion compositions worldwide is the high concentration of Ca, Mg, and Fe compared with Na, K, Al, Si, and Cl (Weiss et al., 2015). We found that the assemblage, olivine ($Fo_{90}Fa_{10}$), spinel (0.80), carbonate solid-solution ($Cal_{65.5}Mgs_{28.6}Sd_{5.9}$), and diamond could be in equilibrium with such a fluid, where Cal, Mgs, and Sd represents the calcite, magnesite, and siderite components, respectively of the carbonate mineral solid-solution (Whitney and

Table 2
Calculated model compositions (molal), and $logf_{O_2}$ and pH values of the three end-member fluids involved in Panda diamond formation and the mineral compositions used to compute the fluid chemistry. Numbers in parentheses are the activities of the solid solution components based on the ideal site-mixing approximation with one mole of cation per site.

	Peridotitic fluid[a]		**Eclogitic fluid**[b]		**Carbonated dunitic fluid**[c]	
Variable	Concentration	Set with	Concentration	Set with	Concentration	Set with
K	4.0	Phlogopite (1.0)	0.70	Given	0.40[d]	Given
Na	2.0[d]	Given	0.41	Jadeite (0.07)	0.40[d]	Given
Ca	0.63	Grossular (0.10)	0.50	Diopside (0.67)	2.8	Calcite (0.286)
Mg	0.44	Forsterite (0.92)	0.32	Pyrope (0.32)	1.5	Magnesite (0.655)
Fe	0.82	Fayalite (0.08)	0.50	Almandine (0.50)	1.7	Fayalite (0.10)
Al	0.039	Pyrope (0.80)	0.25	Grossular (0.18)	0.14	Spinel (0.80)
Si	0.71	Enstatite (0.955)	6.2	Coesite (1.0)	0.56	Forsterite (0.90)
C	9.4	Diamond (1.0)	3.0	Diamond (1.0)	7.9	Diamond (1.0)
Cl	8.0	Given	1.0	Given	1.0	Given
pH	4.48	Charge Balance	4.76	Charge Balance	5.24	Charge Balance
a_{H_2O}	0.72		0.86		0.82	
$logf_{O_2}$[e]	−12.3		−11.6		−10.6	
$logf_{O_2} - QFM$	−3.9		−3.2		−2.2	

[a] Averaged values of mineral inclusions in peridotitic diamonds (Tomlinson et al., 2006). Phlogopite was assumed in equilibrium with the fluid to give an upper limit for K.
[b] Averaged values of mineral inclusions in eclogitic diamonds (Stachel and Harris, 2008).
[c] A model metasomatized, carbonated peridotite assemblage assumed to fit to end-member low Mg-carbonatitic Panda fluid.
[d] Approximated from fluid inclusion end-member data.
[e] logfo$_2$ for each fluid a fit parameter (see text). In the final row, the values are also expressed relative to the theoretical value for the QFM buffer at 4.5 GPa and 950 °C (−8.4) calculated using the Deep Earth Water model.

Evans, 2010). This mineral assemblage could correspond to a carbonated dunite.

Spinel compositions reported as xenocrysts from the Slave craton vary widely from about 12 to 65 wt.% Cr_2O_3 (Griffin et al., 1999). Spinel grains reported as inclusions in diamond, however, are uniformly Cr-rich, typically about 65 wt% Cr_2O_3 (Tappert et al., 2005). For reference, pure $MgCr_2O_4$ contains 79.0 wt% Cr_2O_3. These observations suggest that Al-bearing spinel containing Cr may be transformed into very Cr-rich spinels (Mg-chromites) during diamond formation. Consequently, for the carbonatitic fluid source rock, we used a spinel with a substantial activity of $MgAl_2O_4$ equal to 0.80. We had not yet explicitly include Cr in the model because chemical analyses for aqueous Cr in the fluid inclusions were not reported by Tomlinson et al. (2006).

The above mineral components were used to constrain the fluid speciation and solubility model, assuming ideal site-mixing. In addition, we assumed values for the K, Na, and Cl concentrations from the fluid inclusions due to a lack of stable mineral phases hosting these elements. Another assumption in the model involved the third Fe-OH complex. In trial calculations, we found that our predicted values of the total dissolved Fe-content of the carbonatitic fluid were too low. At least one of the Fe-complexes needed to be stronger to fit the fluid inclusion data (or a new complex of some unknown type was needed). The Fe-Cl complexes could not be responsible because the chloride content of the carbonatitic fluid is too low. The $Fe(OH)_3^-$ complex was previously constrained by fitting experimental data (Shock et al., 1997). Fe-carbonate or bicarbonate complexes did not behave in a satisfactory manner. Therefore, given the high pH of the carbonatitic fluid, we strengthened the $logK$ value of the $Fe(OH)_3^-$ complex at 950 °C and 4.5 GPa. It should be noted that this adjustment was also carried over for the other two end-member fluid models. In the absence of additional constraints from experimental studies, this was a reasonable adjustment to make because the equilibrium constant of $Fe(OH)_3^-$ in the DEW model is only constrained by experiments to 300 °C at vapor saturation pressures (Psat). All other metal-hydroxide complexes used for the carbonatitic fluid were predicted in the DEW model. Finally, we obtained the $logf_{O_2}$ by regression and the pH of the fluid was calculated in the aqueous speciation model through charge balance.

3.3. Diamond formation model

Using the model end-member saline and carbonatitic fluids, it becomes possible to simulate diamond formation in the peridotite environment. Because the fluid inclusions from such diamonds contain such a large range of compositions, most dramatically shown by the range of chloride from very saline to dilute, it is crucial to envision a conceptual model that can potentially explain this range of chemistry. The simplest way to explain such a range of chloride is through mixing of fluids. Where this mixing took place is a matter of speculation. However, numerous studies have emphasized diamond formation in subduction-zone settings (Weiss et al., 2015; Smit et al., 2016; Weiss et al., 2016; Li et al., 2019). Consequently, several conceptual models of diamond formation were investigated based on mixing of fluids in a subduction zone setting.

4. RESULTS

4.1. Comparison of end-member fluid compositions from the Panda diamonds with model fluid compositions calculated from mineral assemblages

The three end-member fluid compositions of the Panda diamond fluids established in the present study by extrapolation of fluid inclusion data to low and high chloride concentrations as described above are given in Table 1. Our three model end-member fluids calculated from the mineral assemblages described above are given in Table 2. For each chemical element in Table 2, the mineral component and its activity used to constrain the fluid chemistry are given. A comparison of the natural end-member fluids and the model fluids is plotted in Fig. 2. The solid line with a slope of 1.0 on each plot indicates perfect agreement. It can be seen that, with a few exceptions, notably Si in Fig. 2a, Al in Fig. 2b, and Fe in Fig. 2c, the model peridotitic, eclogitic and carbonated dunitic fluids agree within an uncertainty of ±0.3 log units with the saline, silicic, and carbonatitic end-member fluids determined by extrapolation of the Panda fluid inclusion data, respectively. In the case of Si in Fig. 1a, the discrepancy shown may well be a consequence of the model assumption of equilibrium with coesite, which has not been reported as an inclusion in Panda diamonds. The origin of the discrepancies for Al in Fig. 2b, and Fe in Fig. 2c is not apparent, but may reflect the need for additional aqueous complexes of these elements in the model. Nevertheless, overall, the plots in Fig. 2 re-emphasize the fundamental differences between the three end-member fluids with respect to the elements Na, K, Cl, Mg, Ca, Fe, Al, and Si and support the proposed connection between the measured fluid inclusion major-element compositions and solid inclusion mineral assemblages.

Carbon in the fluid inclusions cannot be measured directly but our model assumption that each fluid was in equilibrium with diamond yields the carbon speciation in

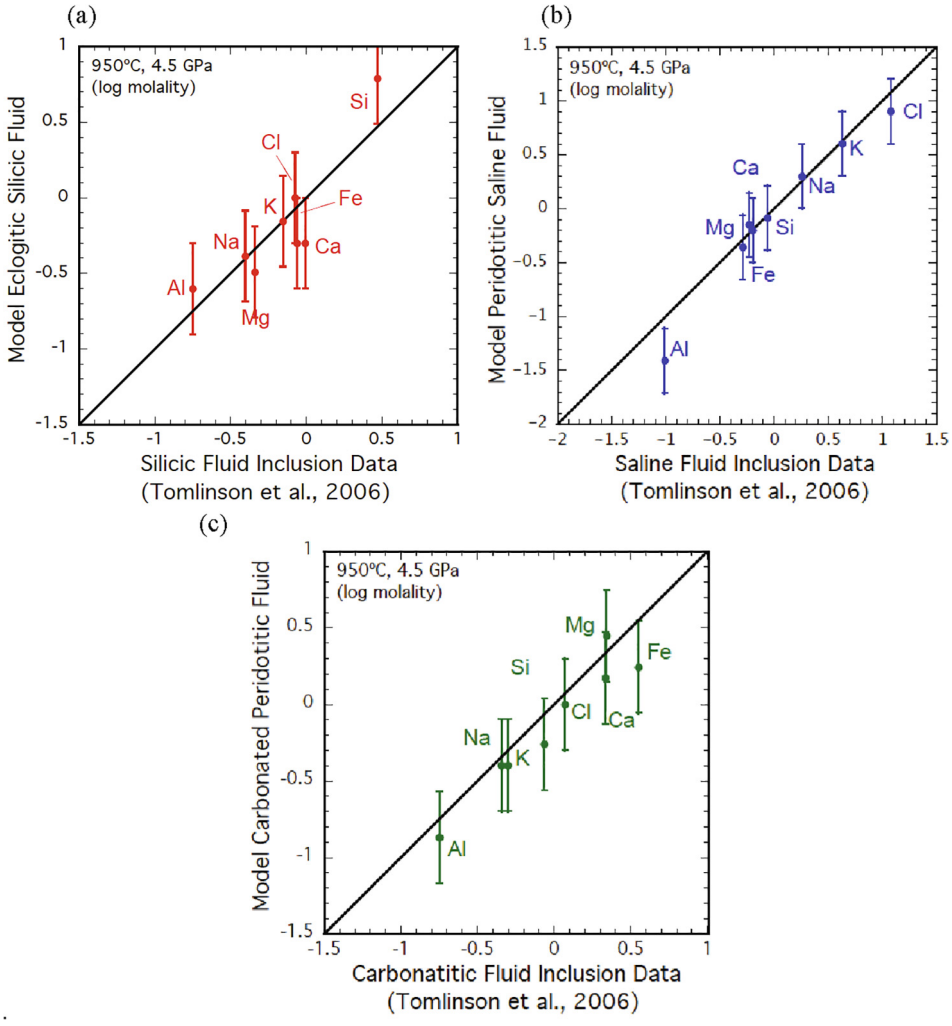

Fig. 2. Comparison of model end-member fluids with extrapolated end-members of fluid inclusions in Panda diamonds: (a) Model fluid in equilibrium with eclogite (silicic fluid); (b) Model fluid in equilibrium with peridotite (saline fluid); (c) Model fluid in equilibrium with carbonated dunite (carbonatitic fluid). Inclusion end-member compositions are given in Table 1, model fluid compositions and speciation in Tables 2 and 3.

the fluid and the total dissolved carbon for given values of the $logf_{O_2}$. Our values of the $logf_{O_2}$ for each fluid-rock system (Table 2) were obtained by fitting the major element data described above. The model concentrations of the major elements depend on f_{O_2} because of the strong metal-formate and metal-bicarbonate complexes in the model, which in turn were independently derived previously by fitting solubility data (Huang and Sverjensky, 2019). The model values of $logf_{O_2}$ relative to QFM are −2.2 to −3.9, which compare favorably with those measured on deep xenoliths from the Diavik diamond mine, −1.0 to −3.8 (Creighton et al., 2010) and +0.03 to −3.73 (Miller et al., 2016). Table 2 also shows the predicted values of the total dissolved C in the fluids and the *pH* values of the fluids. It is notable that the predicted solubility of diamond in these fluids varies from 3.6 to 9. Clearly, diamond-forming fluids can transport very substantial amounts of carbon. Finally, the predicted *pH* values are all alkaline (4.5 to 5.2) compared to neutral *pH* (2.77) under these conditions.

The proportions of groups of elements in the three model fluids are compared with the measured Panda fluid inclusion data in Fig. 3a & b and with the worldwide data in Fig. 3c & d. The model saline and carbonatitic end-member fluids lie almost on the ends of the peridotitic fluid inclusion array (Fig. 3a). The reason that the two points did not fall at the very ends is likely that the mineral compositions used to compute the model fluids were averages rather than extreme values. The eclogitic end-member fluid lies at the very end of the array toward silicic fluid inclusions due to the high Si concentration caused by the presence of coesite in the model. Interestingly, in Fig. 3c and d, the three model fluids also compare well as three end members of fluid inclusions in worldwide diamonds.

4.2. Predicted aqueous speciation in the Panda end-member fluids

The ten most abundant species in the three model fluids are given in Table 3. Organic aqueous species, including methane, ethane, and formate, are predicted to be among the most abundant species in all three fluids. Metal-C complexes, such as $Ca(HCOO)^+$, $Fe(HCOO)^+$ and $Mg(H_4SiO_4)HCO_3^+$, are also very abundant due to the high C concentrations in the fluids (3.0–9.4 molal), and because the systems are in equilibrium with diamond and at appropriate f_{O_2} and *pH* values. Only K and Na have a simple speciation, occurring mainly as the monovalent ions. The elements Mg, Ca, Fe, Al, and Si are all present in the form of metal-C, metal-Si, or metal-OH complexes, whose stabil-

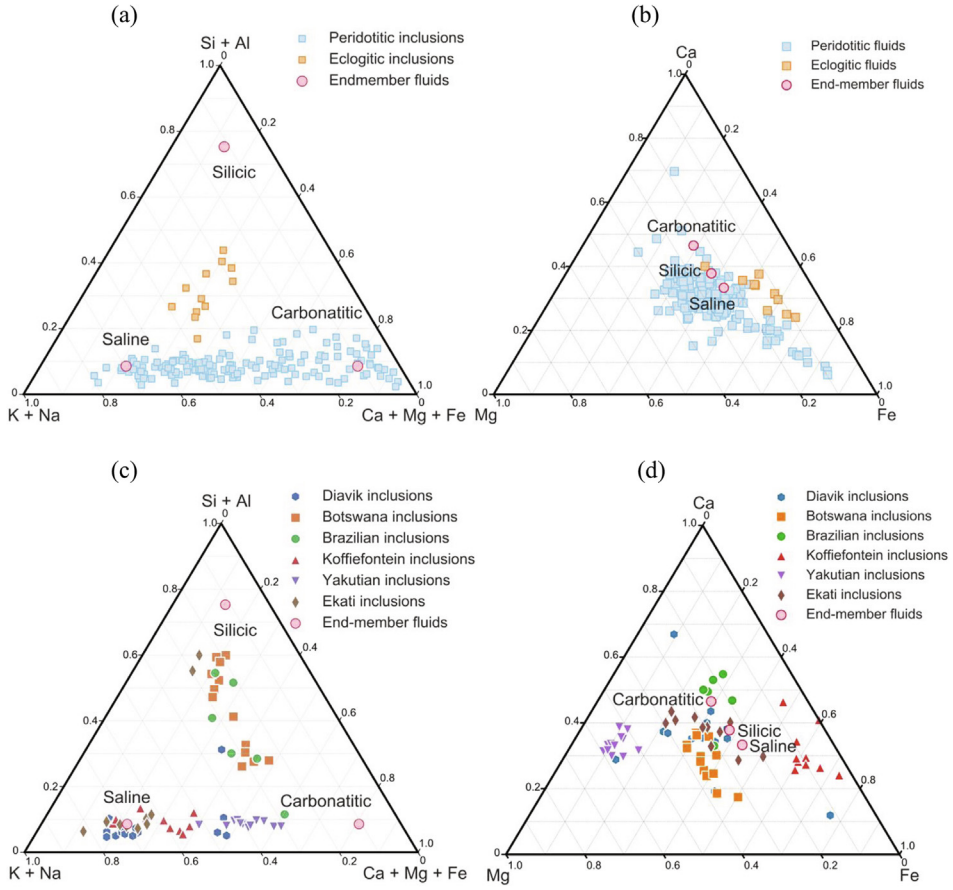

Fig. 3. Grouped major element comparison of model end-member fluids with fluid inclusions from diamonds: (a) and (b) Panda fluid inclusions in diamonds; (c) and (d) Worldwide inclusions in diamonds.

Table 3
Model aqueous speciation results for the ten most abundant aqueous species (molal) and the *pH* and $logf_{O_2}$ values of the three end-member fluids involved in Panda diamond formation at 4.5 GPa and 950 °C.

Model Peridotitic		Model Eclogitic		Model Carbonated Peridotitic	
$CH_4(aq)$	6.1	$H_4SiO_4(aq)$	1.7	$Ca(HCOO)^+$	2.5
Cl^-	5.4	$CH_4(aq)$	1.4	$HCOO^-$	1.4
K^+	3.2	Cl^-	0.94	$H_2CO_3(aq)$	1.3
Na^+	1.5	$H_8Si_3O_{10}(aq)$	0.84	$Mg(OH)_2(aq)$	1.1
$C_2H_6(aq)$	0.93	K^+	0.61	Cl^-	0.96
$KCl(aq)$	0.66	$Ca(H_3SiO_4)^+$	0.40	$Fe(HCOO)^+$	0.90
$FeCl_2(aq)$	0.59	$H_6Si_2O_7(aq)$	0.35	OH^-	0.89
$NaCl(aq)$	0.39	$H_3SiO_4^-$	0.33	$FeO(OH)^-$	0.84
$Mg(OH)_2(aq)$	0.29	Na^+	0.33	$Mg(H_4SiO_4)HCO_3^+$	0.41
$Ca(H_3SiO_4)^+$	0.24	$Fe(HCOO)^+$	0.29	K^+	0.30
pH	4.48		4.76		5.24
$logf_{O_2}$	−12.3		−11.6		−10.6
$logf_{O_2} - QFM$	−3.9		−3.2		−2.2

ities are favored at high temperature, even at high pressure (i.e. 4.5 GPa). These complexes lead to the high solubilities of the major elements (Table 2).

The speciation in the three fluids is different despite the similarities discussed above. In the peridotitic fluid, K^+-Na^+-Cl^--KCl^0 are the major non-C species. The abnormally high *KCl* concentration distinguishes this fluid from other abundant aqueous fluids on and in the Earth, such as meteoric water (Na^+-Cl^-), seawater (Na^+-Mg^{2+}-Cl^--SO_4^{2-}), and hydrothermal fluids (Na^+-Ca^{2+}-Cl^-) in the Earth's crust (Berner and Berner, 2012). The high K appears to reflect the very high solubility of phlogopite in these fluids and the absence of any other minerals in the Panda system that could limit the potassium solubility at this temperature and pressure (Tomlinson et al., 2006). The three major Si species in the peridotitic fluid are $Ca(H_3SiO_4)^+$ (34%), H_4SiO_4(aq) (31%), and $Mg(H_4SiO_4)HCO_3^+$ (18%) i.e. metal-Si complexes play a major role. In contrast, the Si speciation of the eclogitic fluid is dominated by $H_8Si_3O_{10}$ (aq) (40%), H_4SiO_4 (aq) (27%), $H_6Si_2O_7$ (11%), and the Ca-, Mg-, Fe-, and Al-Si complexes only amount to 17%. The high total dissolved silica is due to the equilibrium with coesite, as noted above. The aqueous silica speciation of the carbonated dunitic fluid is similar to that of the peridotitic fluid - the main Si species are metal-Si complexes. In all three models, the major elements mainly appear as complexes, and the types of complexes depend on the oxygen fugacity, the Si and C concentrations, and the *pH* of the fluids.

4.3. Predicted mineralogical changes during diamond formation

In this section, the results of the chemical mass transfer calculations for our conceptual model of diamond formation are described. Our preferred, reference conceptual model of diamond formation involves a carbonatitic fluid originating from a subducting slab infiltrating a harzburgitic environment (Fig. 4). The carbonatitic fluid is assumed to have the composition established above. The harzburgitic environment is assumed to consist of an excess amount of olivine, orthopyroxene, and garnet and the saline pore fluid established above, as summarized in Table 4. The maximum ratio of carbonatitic to saline fluids was 10 to 1. In this scenario, it can be expected that the chloride content of the fluid in the peridotitic environment, although initially high, will decline because of extensive mixing with the invading carbonatitic fluid. If diamond forms under these circumstances, it can be expected to contain inclusions that are zoned from high salinity in the core of a diamond crystal to lower salinity at the edges. Zonation of Cl, consistent with these predictions, has been observed in diamonds in two studies (Klein-BenDavid et al., 2004; Weiss et al., 2014). We carried out our diamond formation modeling using the EQ3/6 package with the temperature and pressure of the system set at 950 °C and 4.5 GPa, while the oxygen fugacity and *pH* are determined throughout by the bulk chemistry of the reacting system. All the minerals and the fluid mixing are assumed to have the same relative reaction rates, which may be a reasonable assumption at the elevated temperature and pressure of the Panda diamond formation.

The initial harzburgitic reactant minerals olivine, garnet, and orthopyroxene are progressively destroyed during reaction progress as the fluids mix. Each unit of the reaction progress variable (ξ) corresponds to destruction of 1.0 mole of each of the reactant minerals and mixing with carbonatitic fluid containing 1.0 kg of H_2O. The new minerals formed are plotted in Fig. 5a - e as functions of the logarithm of the reaction progress variable (logξ). It can be seen in Fig. 5a that the model results are plotted to a logξ value of +0.50 where the three mineral inclusion types in the Panda diamonds are all in equilibrium with diamond, i.e. clinopyroxene, olivine, garnet. We chose this point for comparison with the Panda diamonds because after this point of reaction progress, clinopyroxene disappears and the compositions of the olivines and garnets evolve past the Panda samples. It can also be seen in Fig. 1a that diamond formed and persisted throughout the full extent of reaction progress shown. On a molar basis diamond becomes the most abundant mineral formed due to the very high carbon content in the fluids. However, on a volume basis, assuming

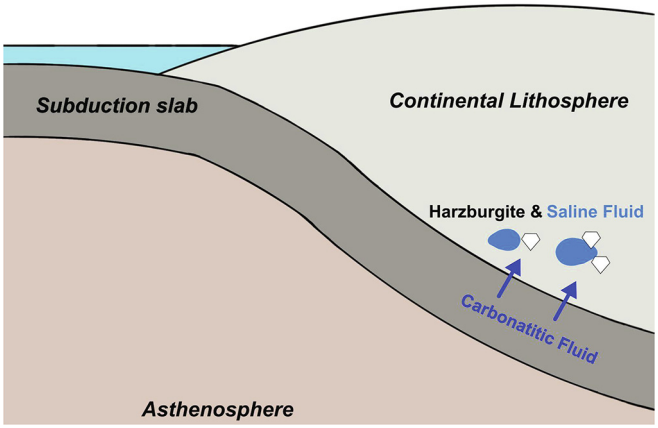

Fig. 4. Conceptual model for diamond formation. Preferred reference model in which carbonatitic fluid invades saline fluid and harzburgite.

Table 4
Initial and final states for the reaction path model of a carbonatitic fluid invading a harzburgite and simultaneously mixing with a saline peridotitic fluid. Numbers in parentheses are the activities of the solid solution components based on the ideal site-mixing approximation with one mole of cation per site.

Fluid Compositions (Molality)				Rock Compositions (moles or fraction)			
	Initial Carbonatitic[a]	Initial Saline[a]	Final Fluid[b]	Initial Harzburgite[c]		Final Rock[d]	
K	0.40	4.23	1.19			Diamond	13.8
Na	0.4	2.0	0.73	Olivine	30	Olivine	9.033
Ca	2.82	0.71	1.94	*Forsterite*	0.92	*Forsterite*	0.856
Mg	1.49	0.59	0.93	*Fayalite*	0.08	*Fayalite*	0.144
Fe	1.75	0.78	1.20	Orthopyroxene	30	Clinopyroxene	0.1330
Al	0.11	0.05	0.12	*Enstatite*	0.955	$CaSiO_3$	0.464
Si	0.56	0.86	0.57	*Ferrosilite*	0.045	$MgSiO_3$	0.507
C	7.93	9.4	4.64			$FeSiO_3$	0.0287
Cl	1.0	8.0	2.50	Garnet	30	Garnet	3.077
pH	5.24	4.48	5.06	*Pyrope*	0.80	*Pyrope*	0.520
$logf_{O_2}$	−10.6	−12.3	−11.2	*Almandine*	0.10	*Almandine*	0.124
$logf_{O_2} - QFM$	− 2.2	−3.9	−2.8	*Grossular*	0.10	*Grossular*	0.356

[a] Compositions of the initial carbonatitic fluid and the saline fluid (Table 2).
[b] Compositions of the final fluid after reaction of carbonatitic fluid with saline fluid and harzburgite at $log\xi = 0.5$ extent.
[c] Moles of initial harzburgitic minerals and their compositions as mole fractions.
[d] Moles of final minerals and compositions as mole fractions after reaction of carbonatitic fluid with saline fluid and harzburgite.

volumes at ambient conditions of 25 °C and 1.0 bar, olivine and garnet are more abundant than diamond.

The changes in the components of the olivine and garnet solid solutions are shown as functions of reaction progress in Fig. 5b, c, d, and e. The forsterite component of olivine decreases from a mole fraction of 0.90 to 0.86, i.e. it becomes more Fe-rich. Garnet changes from $Prp_{79}Alm_{10}Grs_{11}$ to $Prp_{52}Alm_{12}Grs_{36}$ with reaction progress, i.e. it becomes more Ca and Fe-rich. In order to show these changes more clearly, the predicted Ca/Mg and Fe/Mg ratios are plotted in Fig. 5d. The trends in these ratios are qualitatively consistent with trends of *Ca* and *Fe* enrichment recorded in diamonds measured by Tomlinson et al. (2006).

A more quantitative comparison is shown as part of a triangular plot in the system Ca-Mg-Fe in Fig. 5e. Here it can be seen that the predicted olivine and garnet compositions define trends that overlap well with those of the Panda inclusions. The model trends extend beyond the data from the Panda inclusions, which may indicate that the metasomatism recorded in the diamonds represents only part of a potentially much greater extent of reaction output by the model. Overall, the good agreement where the model trend overlaps the trend of the inclusion data indicates that the assumption of ideal site-mixing is adequate for olivine and garnet. However, the assumption of ideal site-mixing was not adequate for prediction of the peridotitic clinopyroxene compositions. Better clinopyroxene compositions resulted using a solid solution model for clinopyroxene in which the diopside, hedenbergite, and clinoenstatite components were mixed with activity coefficients of 0.4, 0.4, and 0.2, respectively, in order to give less Mg-rich compositions. Using this model, the predicted clinopyroxene produced during the reaction path model changed from $Wo_{35}Fs_{01}En_{64}$ to $Wo_{46}Fs_{03}En_{51}$ (Fig. 5e). The latter final clinopyroxene composition agrees well with the peridotitic clinopyroxene inclusion compositions reported for the Panda diamonds (Fig. 5e).

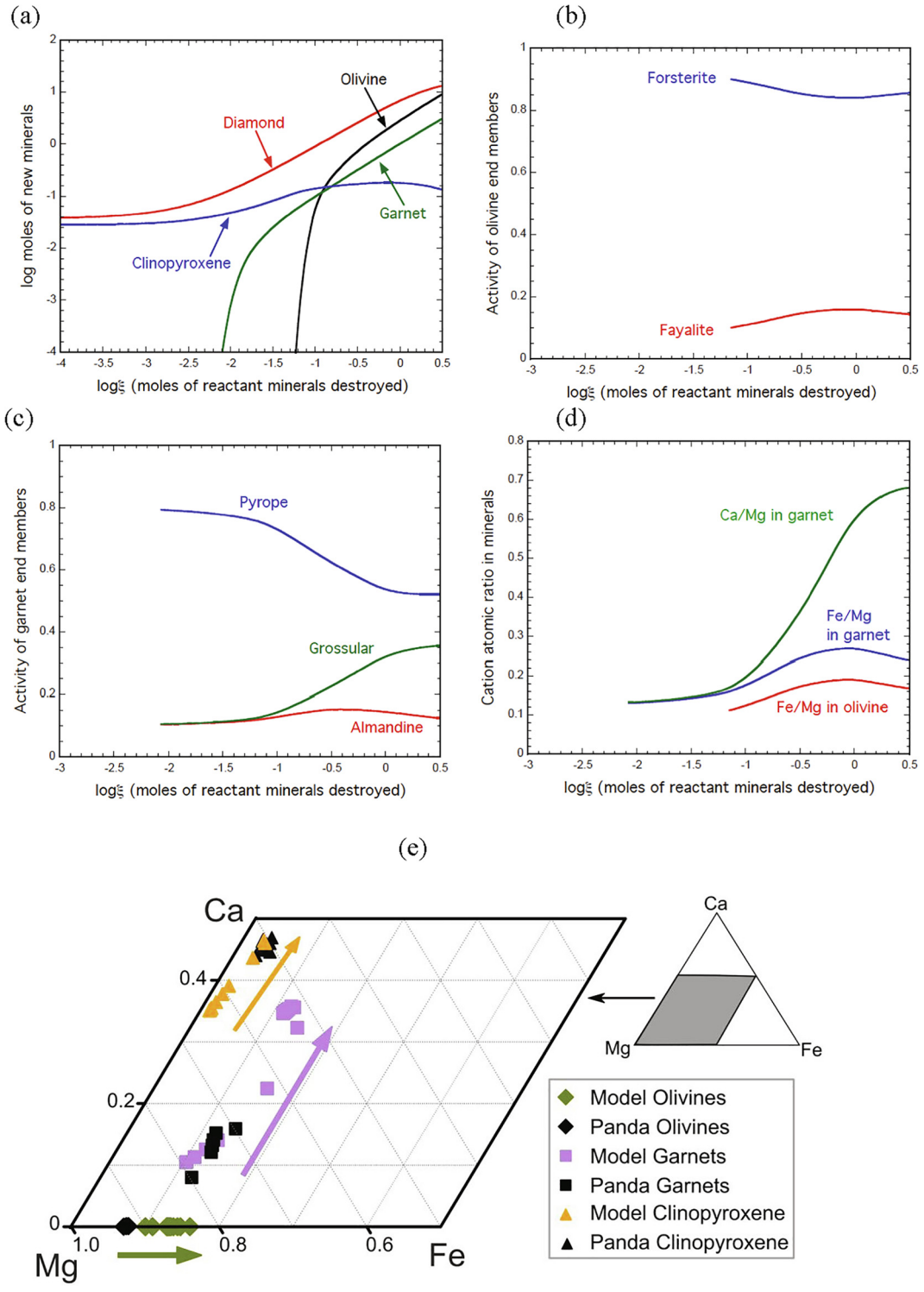

Fig. 5. Predicted mineral evolution as a function of reaction progress during infiltration of the carbonatitic fluid into a saline fluid plus harzburgitic rock: (a) Minerals produced; (b) Olivine solid solutions, (c) Garnet solid solutions, (d) Ca/Mg and Fe/Mg ratios in olivine and garnet; (e) Predicted mineral chemistry versus Panda solid inclusion compositions.

4.4. Fluid evolution during diamond formation

The corresponding changes in the predicted fluid composition in the mass transfer calculations are plotted in Figs. 6 and 7. By simulating the carbonatitic fluid infiltrating the saline fluid plus harzburgite, the fluid composition in the harzburgite environment at the site of diamond formation evolves dramatically. For example, it can be seen

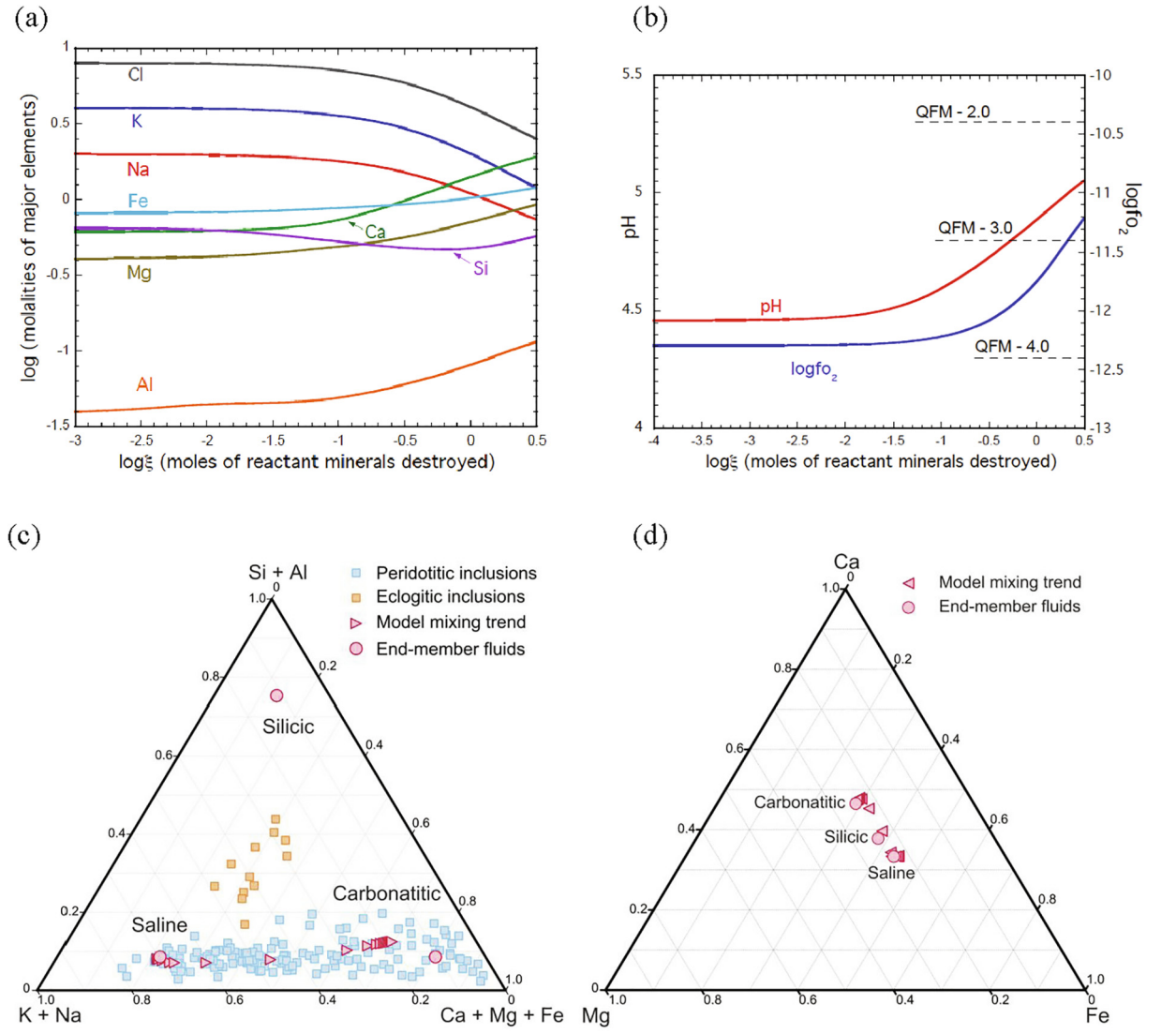

Fig. 6. Predicted fluid evolution as a function of reaction progress during infiltration of the carbonatitic fluid into a saline fluid plus harzburgitic rock. (a) Elemental concentrations in the fluid. (b) pH and logfo$_2$ of the system versus reaction progress (neutral pH is 2.8 and QFM is −8.4 under the model conditions; (c) and (d) Fluid evolution compared to fluid inclusion compositions by atomic proportions.

in Fig. 6a that the total concentrations of elements defining the salinity of the peridotitic fluid, i.e. K, Na, and Cl, decrease dramatically while diamond is forming. Simultaneously, the Ca and Mg contents of the fluid increase. Predicted changes in the *pH* of the fluid at the site of mixing and changes in the $logf_{O_2}$ of the reacting system are shown in Fig. 6b. As expected, the *pH* and the $logf_{O_2}$ both increase owing to the influx of the more oxidizing, higher *pH*, carbonatitic fluid as it mixes into the saline fluid at the site of diamond formation.

The predicted changes in fluid chemistry are shown as reaction paths in Fig. 6c and d in comparison to the measured fluid inclusion data for the Panda diamonds. The overall agreement of the predicted trend of the evolving fluid chemistry agrees well with the measured fluid inclusion compositions of the Panda diamonds. Therefore, the wide range of fluid inclusion compositions for Panda diamonds lying between the saline and carbonatitic end members can be well accounted for by the mixing model proposed above.

Changes in the dissolved carbon species of the evolving fluid at the site of diamond formation are shown in Fig. 7a and b. Although the initial saline fluid associated with the early-formed diamond has a C-speciation dominated by methane and ethane, it can be seen in Fig. 7a that these species containing reduced carbon are displaced by metal complexes containing much more oxidized carbon (i.e. the Ca- and Fe-formate complexes in which the average carbon oxidation state is +II). The dramatic decreases in all the reduced carbon-bearing species, including the dissolved hydrocarbons methane, ethane, and propane are emphasized in Fig. 7b by the dashed curves. In contrast, the concentrations of species containing carbon in oxidation states greater than zero, are depicted by solid curves, which

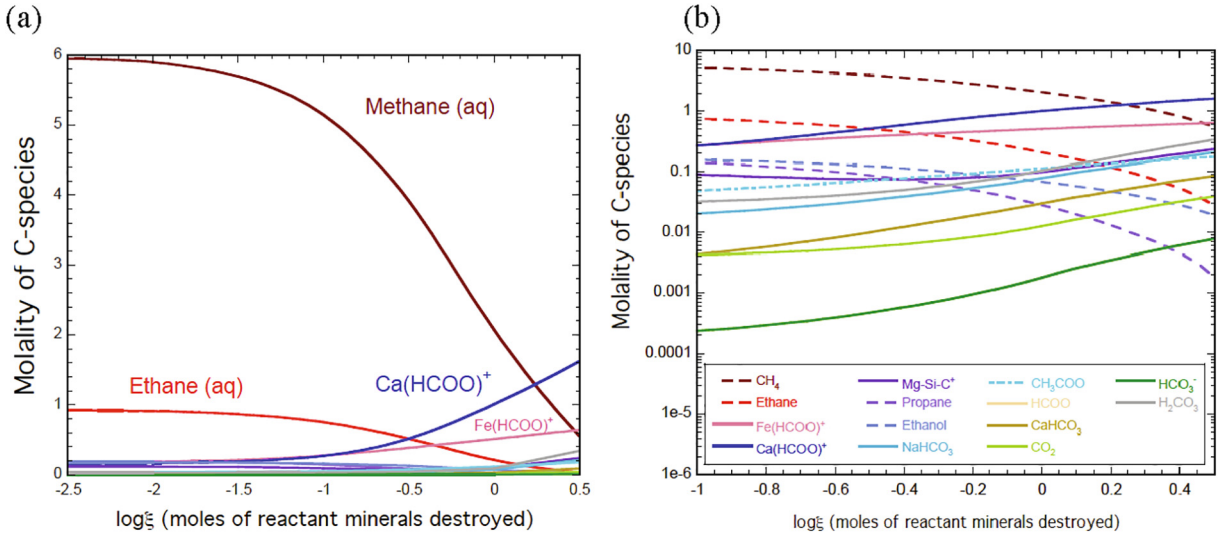

Fig. 7. Predicted fluid C-species during the reaction path calculations as the carbonatitic endmember fluid reacts with a saline fluid plus peridotitic rock environment: (a) The major organic species concentrations in the fluid; (b) An enlarged version on a logarithmic scale of molality showing all the organic species: solid lines for average C valence greater than zero, dashed lines for average C valence less than zero, dot-dashed line for acetate with average C-oxidation state equal to zero.

increase dramatically in the fluids associated with the later-formed diamond. These changes correspond to the increase in $logf_{O_2}$ seen in Fig. 6b. Of all these changes, the drop is greatest for methane - from 6.0 to 0.6 m. However, it should also be noted that, over this range of reaction progress, the methane concentration is being diluted by the carbonatitic fluid. At the same time, formate was added to the system by mixing with the carbonatitic fluid. The sources of carbon going into diamond are discussed in Section 5.3 below.

4.5. Additional models of diamond formation

The simulation results discussed above refer to our reference conceptual model in which a carbonatitic fluid infiltrates the saline fluid in a harzburgitic environment. Simultaneous mixing of the fluids and reaction with the harzburgitic mineral assemblage was observed in the model. Abundant diamond was formed, together with olivine, garnet, and clinopyroxene. These silicate minerals are consistent with the solid inclusions in the coated Panda diamonds reported by Tomlinson et al. (2006). However, one peridotitic Panda diamond studied by Tomlinson et al. (2006) did contain orthopyroxene inclusions, which were not produced in our model. To investigate the sensitivity of our model assumptions, we carried out an additional reaction path simulation in which the incoming carbonatitic fluid only reacted with harzburgite. No saline fluid was present, simulating a dry harzburgite prior to arrival of the carbonatitic fluid. Under these circumstances both orthopyroxene and clinopyroxene formed along with diamond. This scenario is revisited in the discussion section.

We also tested a scenario that could be described as the opposite of our reference model. In this case, the mass transfer calculations used a conceptual model involving a saline fluid, presumably from a subducting slab, infiltrating and mixing with a carbonatitic fluid in a carbonated dunitic environment. This scenario is one that is analogous to that suggested by Weiss et al. (2015). However, in this new scenario, the salinity at the site of diamond formation increases with reaction progress, which is opposite to that observed in the zonation patterns within individual diamonds (Weiss et al., 2015). Furthermore, the Fe content of the olivine and the Ca content of the garnet decreased with reaction progress, again opposite to what is observed in the Panda mineral inclusions (Tomlinson et al., 2006).

5. DISCUSSION

Multiple end-member fluids worldwide have been recognized in the very large range of fluid inclusion compositions in diamonds, indicating a wide range of compositions for mobile phases in the upper mantle (Weiss et al., 2015). However, the origins of these fluids have remained unclear. Similarly, a wide range of origins for diamonds themselves have been suggested, based on the chemical and isotopic characteristics of the diamonds and their mineral inclusions (Shirey et al., 2013; Stachel and Luth, 2015). We have focused on the origin of the fluids recorded in the Panda diamonds studied by Tomlinson et al. (2006), and the possible formation processes for these specific diamonds because the compositions of both fluid and solid inclusions were reported and a clear case for metasomatic activity associated with diamond formation was documented by Tomlinson et al. (2006). We first discuss the results of our study of the fluid inclusions and then the implications of our preferred model for the formation of the Panda diamonds.

5.1. Origins of end-member fluids recorded in Panda fluid inclusions

The results of our study have established that the compositions of the three end-member fluids recorded in fluid inclusions from the Panda diamonds may be the result of equilibration with three upper mantle rock types. The *KCl*-rich, saline end-member fluid is consistent with equilibrium with peridotite, specifically a harzburgite, although it should be noted that the K-content of the fluid is an upper limit based on equilibrium with phlogopite and the Cl-content comes from the reported fluid inclusion compositions. The silicic end-member fluid is consistent with equilibration with a coesite-bearing eclogite. The Ca + Mg + Fe-rich, carbonatitic, end-member fluid could have resulted from equilibration with a carbonated dunite. The suggestion of the involvement of dunite in the generation of diamond-forming fluids is unusual. However, all three rock types, harzburgite, coesite bearing eclogite and carbonated dunite, have been reported as xenoliths in kimberlites from the Slave craton (Griffin et al., 1999). Furthermore, it appears that a distinctive feature of the Slave craton is a relatively shallow (<140 km depth), highly depleted layer in the upper mantle. Xenoliths from this layer are extremely olivine-rich. It has been suggested that this layer was part of a subduction zone that became accreted to the early Slave craton (Griffin et al., 1999; Tappert et al., 2005). Consequently, it is conceivable that early in the development of the Slave craton, carbonatitic fluids could have originated in this layer.

The origin of the high salinity (i.e. high concentrations of K + Na + Cl) in the saline end-member fluid is still enigmatic. Weiss et al. (2015) suggested that this fluid was the parental fluid during diamond formation, with a potential origin as sea water trapped in a subducting slab. However, seawater has a chloride content about sixteen times lower than the saline fluid that we used in our model. Consequently, a highly efficient concentration mechanism would be needed to generate such high salinities from seawater. One possible source of Cl could be the breakdown of a Cl-rich phengite during subduction. Alternatively, a Cl-rich reservoir has been suggested in the deep sub-lithospheric mantle based on isotopic studies of fresh chloride-rich kimberlite from Siberia (Maas et al., 2005). This suggestion has received recent support from experimental studies. Reaction of a natural sample of pelitic sediment with dunite at 5.0 GPa and 1,000 °C has yielded a peridotite containing $(K,Na)Cl$ crystals (Förster et al., 2019) If such a rock could form in nature, it could be a potent source of *KCl* in fluids in the upper mantle.

All three model end-member fluids are rich in carbon and the carbon species in the fluids are predicted to be predominantly organic species with a wide range of oxidation states. As previously noted (Sverjensky et al., 2014c), the traditional C-O-H fluid model only included a few aqueous carbon species, such as CH_4, CO, and CO_2, but many additional species with intermediate oxidation states of the carbon appear to become stable at pressures above about 3.0 GPa (e.g. C in $HCOO^-$ has an oxidation state of + 2.0). In our current DEW model, calibrated with experimental data on peridotite and eclogite solubilities (Kessel et al., 2005; Dvir et al., 2011; Kessel et al., 2015), we included organic species such as $CH_4(aq)$, CO, $HCOO^-$ and metal-formate complexes of Ca and Fe. We did not include $CH_3CH_2COO^-$ in the current model owing to uncertainties in its thermodynamic properties. However, it appears theoretically possible that such longer chain acid anions and hydrocarbons could become stable at high pressures (Sverjensky et al., 2014c). Recent experimental studies are also consistent with the apparent stability of organic species in fluids and the formation of immiscible hydrocarbons at elevated pressures (Huang et al., 2017; Li, 2017). Our models of the end-member fluids represented in fluid inclusions strongly suggest the involvement of organic C-species in diamond formation. This conclusion is supported by recent reports of hydrocarbons and other organic species in fluid inclusions in diamonds as observed at ambient condition temperatures (Frezzotti, 2019; Sobolev et al., 2019).

5.2. Origin of peridotitic Panda diamonds

Building on the models of the end-member saline and carbonatitic fluids from the fluid inclusion study described above, we carried out a detailed simulation of the formation of the peridotitic Panda diamonds. Previously, it was shown that a carbonatitic fluid could react with eclogites to generate diamonds and a spectrum of fluid inclusion compositions between the carbonatitic and eclogitic end-member fluids (Sverjensky and Huang, 2015). In that study, a drop in the pH of the fluid at almost constant $logf_{O_2}$ values caused the precipitation of diamond.

In the present study, we focused on diamond formation in the peridotitic environment by mixing of carbonatitic and saline fluid end members with simultaneous reaction with harzburgite. It was assumed here that the carbonatitic fluid came from a subducting slab. The saline fluid end member was assumed to reside in the harzburgite, with indeterminate origin. It may have a subduction origin, or it may have formed in the upper mantle (as discussed above). Under these circumstances a spectrum of fluid compositions was generated that corresponds closely to measured fluid inclusion compositions. Because the model carbonatitic fluid has a much lower Cl content than the saline fluid, mixing the two fluids is a simple way to generate a wide range of salinities corresponding to that in the fluid inclusions. Furthermore, our model predicts the correct evolution of salinity in the diamond fluid inclusions from saline in the earliest-formed diamond in the core to less saline in the outer parts of a zoned diamond crystal. This predicted spatial zonation is a consequence of our conceptual model (Fig. 4) in which carbonatitic fluid gradually infiltrates a harzburgite containing a saline pore fluid.

In our conceptual model for diamond formation, the earliest formed diamond in such a system is more influenced by the saline fluid and the harzburgite than the infiltrating carbonatitic fluid. With more extensive reaction progress, the carbonatitic fluid has the predominant influence, as indicated by the increase of the Ca and Fe concentrations in olivine and garnet solid inclusions in the fibrous diamonds coating monocrystalline cores. In this regard, our

conceptual model is also consistent with the conclusions of an $^{187}Os/^{188}Os$ isotopic study of diamonds and xenoliths from the Panda kimberlite (Westerlund et al., 2006). There it was found that the extremely unradiogenic harzburgite influenced the isotopic compositions of sulfide inclusions in the earliest-formed diamond. Subsequent sulfide inclusions in diamond recorded the more radiogenic influence of an infiltrating fluid. The consistency of the conclusions from the osmium isotopic study and our reaction path modeling suggests that it is likely that the radiogenic infiltrating fluid corresponds to our carbonatitic fluid. Finally, the chemistry of our carbonatitic fluid is also consistent with an increase in Ca and Fe concentrations in garnet and olivine mineral inclusions in the Panda diamonds from core to rim, consistent with the trend of increased metasomatic activity suggested by Tomlinson et al. (2006).

Based on our studies of carbonatitic fluid invading either eclogite or harzburgite, we suggest that carbonatitic fluids may be the parental fluids for a wide range of diamond formation. This contrasts with the conclusion of Weiss et al. (2016), who suggested that a saline fluid was the parental fluid for diamond formation from Diavik diamond mine. Our model also differs from that of Stachel et al. (2017), who suggested diamond was formed from a single fluid containing a mixture of CH_4 and CO_2. However, it should be emphasized that our carbonatitic fluid is one particular end-member fluid; it is a low-Mg carbonatitic fluid that occurs in the Panda diamond fluid inclusions. Worldwide, there is also a high-Mg carbonatitic fluid, which was not considered here. It is conceivable that a Mg-rich carbonatitic fluid might leave different traces of its passage, not only in the fluid inclusions in diamond, but also in the chemistry of the solid inclusions. For example, very low-Ca garnets have been widely described in harzburgite and dunite xenoliths and in inclusions in diamonds from the South African and Siberian cratons (Boyd et al., 1993; Malkovets et al., 2007) and these may reflect addition of Mg rather than Ca during metasomatism. These are fundamental differences in fluid chemistry and mineral chemistry compared to xenoliths and diamonds from the Panda kimberlite.

Our reference model of diamond formation in the peridotitic environment involving the low-Mg carbonatitic fluid from the Panda diamonds mixed with the saline fluid and reacted with harzburgite accounted for most of the observed characteristics of the Panda diamond formation. However, it did not result in the formation of orthopyroxene, which has been documented as solid inclusions in Panda diamonds. It is possible that the orthopyroxene inclusions in the Panda diamonds are inherited from the pre-existing mantle harzburgite. However, it is also possible that these inclusions formed by a different process of fluid-rock interaction. For example, an additional reaction path simulation was carried out in which the incoming low-Mg carbonatitic fluid only reacted with harzburgite, without any saline fluid present. Under these circumstances, both orthopyroxene and clinopyroxene were observed in the model to form along with diamond. This intriguing result suggests that perhaps some diamond could form in a peridotitic environment that was dry before the arrival of the

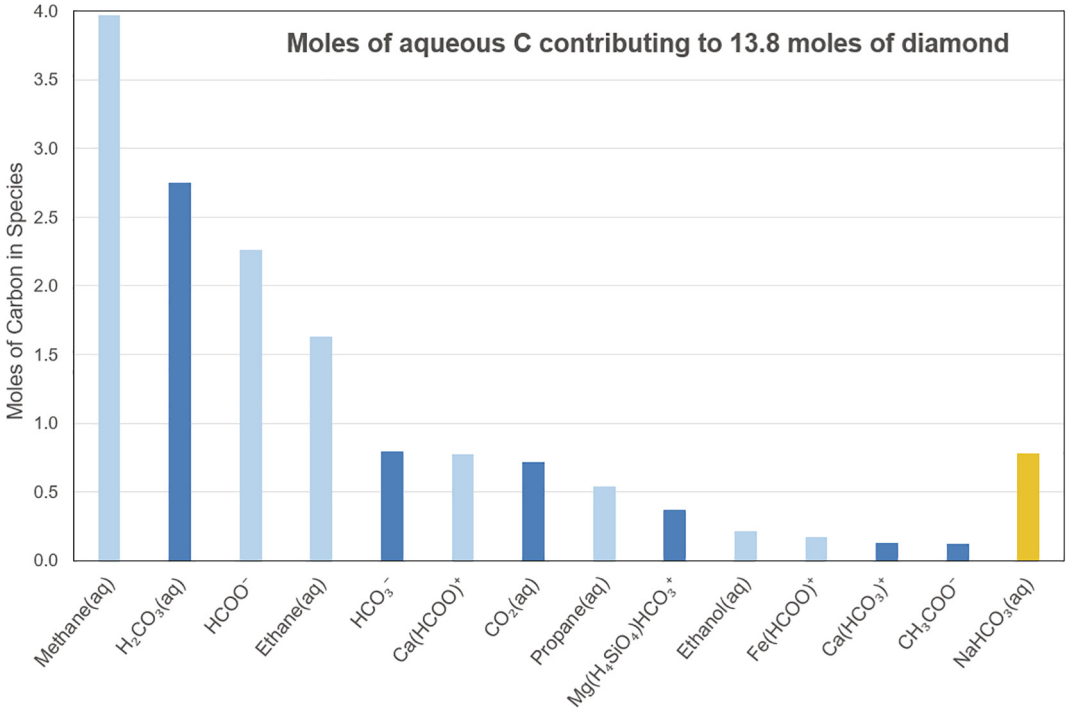

Fig. 8. The carbon budget for the formation of diamonds. Moles of the organic species that contributed to the formation of Panda diamonds. The blue color indicates that the species was consumed and the orange color indicates that it was produced during the fluid mixing process. Among the blue colors, the dark blue refers to species with a positive C-valence and the light blue refers to species with a negative C-valence. (For interpretation of the references to colour in this figure legend, the reader is referred to the web version of this article.)

carbonatitic fluid. Inclusions of orthopyroxene or clinopyroxene in diamond formed in this way might reflect the carbonatitic fluid, but inclusions of minerals from the unaltered harzburgite (i.e. protogenetic) might reflect a locally dry mantle (Novella et al., 2015; Taylor et al., 2016).

5.3. Carbon budget during diamond formation

A topic of great interest in the origin of diamonds is the source or sources of the carbon in the diamonds. Our calculations for the reference model of diamond formation shows dramatic drops in the concentrations of the hydrocarbons – methane, ethane, and propane – at the site of diamond formation. Of all these changes, the drop is greatest for methane - from 9.3 to 4.6 m at $\log\xi = 0.5$, i.e. a 4.7 molal drop. However, it should be noted that, over this range of reaction progress, 3.2 kg of molecular H_2O in carbonatitic fluid was added, so that the actual drop in $CH_4(aq)$ is less than 4.7 molal. Taking this dilution effect into account, it becomes possible to assess how much carbon in diamond came from the different species in the complex mixed fluid.

The amounts of carbon going into the model diamond from the main C-bearing species in the fluid can be evaluated at a specific value of reaction progress. For example, Fig. 8 lists the changes in the total number of moles of C from each of the aqueous species from the beginning of reaction to $log\xi = 0.5$ extent of reaction. These numbers refer to the change in moles of each organic species in the mixed fluid, and sum to the total number of moles of diamond precipitated. In the 13.8 moles of diamond formed, 4 moles came from methane, 2.7 moles from carbonic acid, 2.2 moles from formate, and 1.6 moles from ethane (Fig. 8). These four species account for 76% of the carbon in the diamond. Therefore, the carbon in the diamond comes mainly from oxidation of methane and ethane, and reduction of formate and carbonic acid. Though additional species are clearly involved, examples of simple reactions involving the above species can be written as follows:

$$CH_4 + H_2CO_3^0 = 2C_{diamond} + 3H_2O \quad (1)$$

$$C_2H_6 + 3HCOO^- + 3H^+ = 5C_{diamond} + 6H_2O \quad (2)$$

These reactions are written to illustrate possible pairs of oxidized and reduced carbon reacting to give diamond. Overall, it is clear that a reaction of a suite of oxidized carbon species from the carbonatitic fluid has reacted with a suite of reduced carbon species from the saline fluid to generate diamond. An attractive feature of this model is that the mechanism of diamond precipitation does not call on arbitrary temperature or pressure changes, but instead is a direct consequence of fluid mixing and simultaneous reaction with harzburgite.

6. CONCLUSIONS

We have focused on the origin of the fluids recorded in the Panda diamonds and possible processes of diamond formation in samples studied by Tomlinson et al. (2006) because they reported compositions of both fluid and solid inclusions for these diamonds and a clear case for metasomatic activity associated with diamond formation and the chemical evolution of silicate inclusions. We computed aqueous speciation and solubility models of the chemistry of fluid inclusions in Panda diamonds to investigate the origins of the three end-member compositions in these fluids. Building on these results, we carried out chemical mass transfer calculations simulating the irreversible chemical reactions taking place during the formation of the Panda diamonds. All calculations refer to upper mantle conditions of 950 °C and 4.5 GPa.

The modeling work produced the following findings:

(1) The three end member-fluids in fluid inclusions in Panda diamonds are as follows: i) a *KCl*-rich, saline end-member fluid, consistent with equilibrium with a harzburgite; ii) a silicic end-member fluid, consistent with equilibrium with a coesite-bearing eclogite; and iii) a Ca + Mg + Fe-rich, carbonatitic end-member fluid that may originate from equilibrium with a carbonated dunite.
(2) The predicted solubility of diamond in these fluids varies from 4.6 to 9.3 m. This substantial solubility indicates that diamond-forming fluids can transport very large amounts of carbon in the deep carbon cycle.
(3) The model values of $logf_{O_2}$ in the end-member inclusion fluids relative to QFM are from −3.9 to −2.2, which compare favorably with those measured on deep xenoliths from the Diavik diamond mine. For example, ranges have been reported of −3.8 to −1.0 (Creighton et al., 2010) and −3.73 to + 0.03 (Miller et al., 2016). The predicted *pH* values are all alkaline, 4.48 to 5.24, compared to neutral *pH* (2.77) under the modeled conditions.
(4) Aqueous organic species are predicted to be the among the most abundant species in the fluids. Methane is the most abundant species in the peridotitic fluid, whereas $Ca(HCOO)^+$, $HCOO^-$, and H_2CO_3, and $Mg(OH)_2$ are the most abundant species in the carbonatitic fluid. A wide range of oxidation states of carbon are represented from methane to ethane and propane, and to acetate and formate, and bicarbonate. Only minor amounts of CO_2 are predicted to occur in these fluids compared to other C-species. Instead, H_2CO_3 is the most abundant oxidized C-species.
(5) Mass transfer calculations demonstrate that infiltration by the carbonatitic end-member fluid into a harzburgitic environment, resulting in mixing with a pre-existing saline end-member fluid coupled with simultaneous reaction with harzburgitic minerals, can generate a spectrum of fluid compositions at the site of diamond formation.
(6) The predicted evolution of the fluid chemistry at the site of diamond formation and the mineral chemistry of olivine and garnet formed along with diamond agree well with observations on the composition of Panda diamond fluid and solid inclusions.

(7) Both the *pH* of the aqueous fluid and $logf_{O_2}$ of the system increased during diamond formation, reflecting the influx of the carbonatitic fluid.
(8) The carbon content of the diamond in our reference model is derived from both the carbonatitic fluid and the saline fluid. Formation of the Panda diamonds was a response to mixing of oxidized and reduced carbon-bearing aqueous species during metasomatism, and did not require arbitrary temperature or pressure changes.

Declaration of Competing Interest

The authors declare that they have no known competing financial interests or personal relationships that could have appeared to influence the work reported in this paper.

ACKNOWLEDGEMENTS

This research was supported by grants from the Sloan Foundation through the Deep Carbon Observatory (Reservoirs and Fluxes and Extreme Physics and Chemistry programs), DOE grant DE-FG-02-96ER-14616, and NSF grants EAR 1624325 and ACI 1550346. The authors are grateful for the help and support of the Johns Hopkins University and the Geophysical Laboratory of the Carnegie Institution of Washington and acknowledge helpful discussions with Y. Fei, R. M. Hazen, R. J. Hemley, R. Kessel, S. Lobanov, C. E. Manning, S. Mikhail, O. Navon, S. B. Shirey, C. M. Schiffries, V. Stagno, E. Tomlinson, G. Pearson, Y. Weiss, R. Luth, K. Smit, J. Hao and H. Hu. We particularly wish to thank A. Jones (University College, London) who suggested this study and D. Viete (Johns Hopkins University) for his comments on the manuscript.

APPENDIX A. SUPPLEMENTARY MATERIAL

Supplementary data to this article can be found online at https://doi.org/10.1016/j.gca.2020.06.011.

REFERENCES

Ague J. J. and Nicolescu S. (2014) Carbon dioxide released from subduction zones by fluid-mediated reactions. *Nat. Geosci.* **7**, 355–360.

Barry P., de Moor J., Giovannelli D., Schrenk M., Hummer D., Lopez T., Pratt C., Segura Y. A., Battaglia A. and Beaudry P. (2019) Forearc carbon sink reduces long-term volatile recycling into the mantle. *Nature* **568**, 487–492.

Berner E. K. and Berner R. A. (2012) *Global environment: water, air, and geochemical cycles*. Princeton University Press.

Boyd F., Pearson D., Nixon P. and Mertzman S. (1993) Low-calcium garnet harzburgites from southern Africa: their relations to craton structure and diamond crystallization. *Contrib. Miner. Petrol.* **113**, 352–366.

Brovarone A. V., Martinez I., Elmaleh A., Compagnoni R., Chaduteau C., Ferraris C. and Esteve I. (2017) Massive production of abiotic methane during subduction evidenced in metamorphosed ophicarbonates from the Italian Alps. *Nat. Commun.* **8**, 14134.

Bureau H., Frost D. J., Bolfan-Casanova N., Leroy C., Esteve I. and Cordier P. (2016) Diamond growth in mantle fluids. *Lithos* **265**, 4–15. https://doi.org/10.1016/j.lithos.2016.10.004.

Bureau H., Remusat L., Esteve I., Pinti D. L. and Cartigny P. (2018) The growth of lithospheric diamonds. *Sci. Adv.* **4**, eaat1602.

Carlson R. W., Pearson D. G. and James D. E. (2005) Physical, chemical, and chronological characteristics of continental mantle. *Rev. Geophys.* **43**.

Connolly J. A. and Galvez M. E. (2018) Electrolytic fluid speciation by Gibbs energy minimization and implications for subduction zone mass transfer. *Earth Planet. Sci. Lett.* **501**, 90–102.

Creaser R. A., Grütter H., Carlson J. and Crawford B. (2004) Macrocrystal phlogopite Rb–Sr dates for the Ekati property kimberlites, Slave Province, Canada: evidence for multiple intrusive episodes in the Paleocene and Eocene. *Lithos* **76**, 399–414.

Creighton S., Stachel T., Eichenberg D. and Luth R. W. (2010) Oxidation state of the lithospheric mantle beneath Diavik diamond mine, central Slave craton, NWT, Canada. *Contrib. Miner. Petrol.* **159**, 645–657.

Duan Z. and Zhang Z. (2006) Equation of state of the H2O, CO2, and H2O–CO2 systems up to 10 GPa and 2573.15 K: molecular dynamics simulations with ab initio potential surface. *Geochim. Cosmochim. Acta* **70**, 2311–2324.

Dvir O. and Kessel R. (2017) The effect of CO2 on the water-saturated solidus of K-poor peridotite between 4 and 6GPa. *Geochim. Cosmochim. Acta* **206**, 184–200.

Dvir O., Pettke T., Fumagalli P. and Kessel R. (2011) Fluids in the peridotite–water system up to 6 GPa and 800°C: new experimental constrains on dehydration reactions. *Contrib. Miner. Petrol.* **161**, 829–844.

Förster M. W., Foley S. F., Marschall H. R., Alard O. and Buhre S. (2019) Melting of sediments in the deep mantle produces saline fluid inclusions in diamonds. *Sci. Adv.* **5**, eaau2620.

Frezzotti M. L. (2019) Diamond growth from organic compounds in hydrous fluids deep within the Earth. *Nat. Commun.* **10**, 1–8.

Galvez M. E., Connolly J. A. and Manning C. E. (2016) Implications for metal and volatile cycles from the pH of subduction zone fluids. *Nature* **539**, 420.

Griffin W., Doyle B., Ryan C., Pearson N., Suzanne Y. O. R., Davies R., Kivi K., Van Achterbergh E. and Natapov L. (1999) Layered mantle lithosphere in the Lac de Gras area, Slave craton: composition, structure and origin. *J. Petrol.* **40**, 705–727.

Huang F., Daniel I., Cardon H., Montagnac G. and Sverjensky D. A. (2017) Immiscible hydrocarbon fluids in the deep carbon cycle. *Nat. Commun.* **8**.

Huang F. and Sverjensky D. A. (2019) Extended Deep Earth Water Model for predicting major element mantle metasomatism. *Geochim. Cosmochim. Acta* **254**, 192–230.

Izraeli E. S., Harris J. W. and Navon O. (2001) Brine inclusions in diamonds: a new upper mantle fluid. *Earth Planet Sc Lett* **187**, 323–332.

Izraeli E. S., Harris J. W. and Navon O. (2004) Fluid and mineral inclusions in cloudy diamonds from Koffiefontein, South Africa. *Geochim. Cosmochim. Acta* **68**, 2561–2575.

Jablon B. M. and Navon O. (2016) Most diamonds were created equal. *Earth Planet. Sci. Lett.* **443**, 41–47.

Kessel R., Pettke T. and Fumagalli P. (2015) Melting of metasomatized peridotite at 4–6 GPa and up to 1200° C: an experimental approach. *Contrib. Miner. Petrol.* **169**, 1–19.

Kessel R., Ulmer P., Pettke T., Schmidt M. and Thompson A. (2005) The water–basalt system at 4 to 6 GPa: phase relations

and second critical endpoint in a K-free eclogite at 700 to 1400 C. *Earth Planet. Sci. Lett.* **237**, 873–892.
Klein-BenDavid O., Izraeli E. S., Hauri E. and Navon O. (2004) Mantle fluid evolution - a tale of one diamond. *Lithos* **77**, 243–253.
Klein-BenDavid O., Izraeli E. S., Hauri E. and Navon O. (2007) Fluid inclusions in diamonds from the Diavik mine, Canada and the evolution of diamond-forming fluids. *Geochim. Cosmochim. Acta* **71**, 723–744.
Klein-BenDavid O., Logvinova A. M., Schrauder M., Spetius Z. V., Weiss Y., Hauri E. H., Kaminsky F. V., Sobolev N. V. and Navon O. (2009) High-Mg carbonatitic microinclusions in some Yakutian diamonds—a new type of diamond-forming fluid. *Lithos* **112**, 648–659.
Klein-BenDavid O., Pearson D. G., Nowell G. M., Ottley C., McNeill J. C. R. and Cartigny P. (2010) Mixed fluid sources involved in diamond growth constrained by Sr–Nd–Pb–C–N isotopes and trace elements. *Earth Planet. Sci. Lett.* **289**, 123–133.
Klein-BenDavid O., Pearson D. G., Nowell G. M., Ottley C., McNeill J. C. R., Logvinova A. and Sobolev N. V. (2014) The sources and time-integrated evolution of diamond-forming fluids – Trace elements and isotopic evidence. *Geochim. Cosmochim. Acta* **125**, 146–169.
Krogh E. (1988) The garnet-clinopyroxene Fe-Mg geothermometer — a reinterpretation of existing experimental data. *Contr. Mineral. Petrol.* **99**, 44–48.
Li K., Li L., Pearson D. G. and Stachel T. (2019) Diamond isotope compositions indicate altered igneous oceanic crust dominates deep carbon recycling. *Earth Planet. Sci. Lett.* **516**, 190–201.
Li Y. (2017) Immiscible C-H-O fluids formed at subduction zone conditions. *Geochem. Pespect. Lett.* **3**, 12–21.
Maas R., Kamenetsky M. B., Sobolev A. V., Kamenetsky V. S. and Sobolev N. V. (2005) Sr, Nd, and Pb isotope evidence for a mantle origin of alkali chlorides and carbonates in the Udachnaya kimberlite, Siberia. *Geology* **33**, 549–552.
Malaspina N., Scambelluri M., Poli S., Van Roermund H. L. M. and Langenhorst F. (2010) The oxidation state of mantle wedge majoritic garnet websterites metasomatised by C-bearing subduction fluids. *Earth Planet. Sci. Lett.* **298**, 417–426.
Malkovets V., Griffin W., O'Reilly S. and Wood B. (2007) Diamond, subcalcic garnet, and mantle metasomatism: Kimberlite sampling patterns define the link. *Geology* **35**, 339–342.
Manning C. E. (2014) Geochemistry: A piece of the deep carbon puzzle. *Nat. Geosci.* **7**, 333.
Menzies M. and Hawkesworth C. (1986) *Mantle metasomatism. United States*. Academic Press Inc, Orlando, FL, USA.
Mikhail S. and Sverjensky D. A. (2014) Nitrogen speciation in upper mantle fluids and the origin of Earth's nitrogen-rich atmosphere. *Nat. Geosci.* **7**, 816–819.
Miller C. E., Kopylova M. and Smith E. (2014) Mineral inclusions in fibrous diamonds: constraints on cratonic mantle refertilization and diamond formation. *Mineral. Petrol.* **108**, 317–331.
Miller W. G., Holland T. J. and Gibson S. A. (2016) Garnet and spinel oxybarometers: new internally consistent multi-equilibria models with applications to the oxidation state of the lithospheric mantle. *J. Petrol.* **57**, 1199–1222.
Navon O. (1999) Diamond formation in the Earth's mantle. In *Proceedings of the 7th International Kimberlite Conference. Cape Town: Red Roof Design*, pp. 584–604.
Nestola F., Jung H. and Taylor L. A. (2017) Mineral inclusions in diamonds may be synchronous but not syngenetic. *Nat. Commun.* **8**, 14168.
Nimis P. and Taylor W. R. (2000) Single clinopyroxene thermobarometry for garnet peridotites. Part I. Calibration and testing of a Cr-in-Cpx barometer and an enstatite-in-Cpx thermometer. *Contr. Mineral. Petrol.* **139**, 541–554.
Novella D., Bolfan-Casanova N., Nestola F. and Harris J. W. (2015) H 2 O in olivine and garnet inclusions still trapped in diamonds from the Siberian craton: Implications for the water content of cratonic lithosphere peridotites. *Lithos* **230**, 180–183.
O'Reilly S. Y. and Griffin W. (2013) Mantle metasomatism, Metasomatism and the chemical transformation of rock. *Springer*, 471–533.
Pan D. and Galli G. (2016) The fate of carbon dioxide in water-rich fluids under extreme conditions. *Sci. Adv.* **2**, e1601278.
Pearson D. and Wittig N. (2008) Formation of Archaean continental lithosphere and its diamonds: the root of the problem. *J. Geol. Soc.* **165**, 895–914.
Piccoli F., Brovarone A. V., Beyssac O., Martinez I., Ague J. J. and Chaduteau C. (2016) Carbonation by fluid-rock interactions at high-pressure conditions: Implications for carbon cycling in subduction zones. *Earth Planet. Sci. Lett.* **445**, 146–159.
Plümper O., John T., Podladchikov Y. Y., Vrijmoed J. C. and Scambelluri M. (2017) Fluid escape from subduction zones controlled by channel-forming reactive porosity. *Nat. Geosci.* **10**, 150.
Sanchez-Valle C. (2013) Structure and thermodynamics of subduction zone fluids from spectroscopic studies. *Rev. Mineral. Geochem.* **76**, 265–309.
Scambelluri M. and Philippot P. (2001) Deep fluids in subduction zones. *Lithos* **55**, 213–227.
Schrauder M., Koeberl C. and Navon O. (1996) Trace element analyses of fluid-bearing diamonds from Jwaneng, Botswana. *Geochim. Cosmochim. Acta* **60**, 4711–4724.
Shirey S. B., Cartigny P., Frost D. J., Keshav S., Nestola F., Nimis P., Pearson D. G., Sobolev N. V. and Walter M. J. (2013) Diamonds and the geology of mantle carbon. *Rev Mineral Geochem* **75**, 355–421.
Shiryaev A. A., Izraeli E. S., Hauri E. H., Zakharchenko O. D. and Navon O. (2005) Chemical, optical and isotopic investigation of fibrous diamonds from Brazil. *Russ Geol Geophys+* **46**, 1185–1201.
Shock E. L., Sassani D. C., Willis M. and Sverjensky D. A. (1997) Inorganic species in geologic fluids: Correlations among standard molal thermodynamic properties of aqueous ions and hydroxide complexes. *Geochim. Cosmochim. Acta* **61**, 907–950.
Smit K. V., Shirey S. B., Stern R. A., Steele A. and Wang W. (2016) Diamond growth from C-H–N–O recycled fluids in the lithosphere: Evidence from CH 4 micro-inclusions and δ 13 C–δ 15 N–N content in Marange mixed-habit diamonds. *Lithos* **265**, 68–81.
Sobolev N. V., Tomilenko A. A., Bul'bak T. A. and Logvinova A. M. (2019) Composition of hydrocarbons in diamonds, garnet, and olivine from diamondiferous peridotites from the udachnaya pipe in Yakutia, Russia. *Engineering*.
Stachel T., Chacko T. and Luth R. (2017) Carbon isotope fractionation during diamond growth in depleted peridotite: Counterintuitive insights from modelling water-maximum CHO fluids as multi-component systems. *Earth Planet. Sci. Lett.* **473**, 44–51.
Stachel T. and Harris J. (2008a) The origin of cratonic diamonds-constraints from mineral inclusions. *Ore Geol. Rev.* **34**, 5–32.
Stachel T. and Harris J. W. (2008b) The origin of cratonic diamonds — Constraints from mineral inclusions. *Ore Geol. Rev.* **34**, 5–32.
Stachel T. and Luth R. (2015) Diamond formation—Where, when and how? *Lithos* **220**, 200–220.
Sverjensky D. A., Harrison B. and Azzolini D. (2014a) Water in the deep Earth: the dielectric constant and the solubilities of quartz

and corundum to 60 kb and 1,200°C. *Geochim. Cosmochim. Acta* **129**, 125–145.

Sverjensky D. A. and Huang F. (2015) Diamond formation due to a pH drop during fluid-rock interactions. *Nat. Commun.* **6**.

Sverjensky D. A., Stagno V. and Huang F. (2014) Important role for organic carbon in subduction-zone fluids in the deep carbon cycle. *Nat. Geosci.* **7**, 909–913.

Sverjensky D. A., Vitale Brovarone A. and Daniel I. (2020) The changing character of carbon in fluids with pressure: Organic geochemistry of Earth's upper mantle fluids. In *Earth's Interior, Geophysical Monograph 249* (eds. Craig E. Manning, J.-F. Lin and Wendy L. Mao). American Geophysical Union Monograph.

Tappert R., Stachel T., Harris J. W. and Shimizu N. (2005) Mineral inclusions in diamonds from the Panda kimberlite, Slave Province, Canada. *Eur. J. Mineral.* **17**, 423–440.

Taylor L. A., Logvinova A. M., Howarth G. H., Liu Y., Peslier A. H., Rossman G. R., Guan Y., Chen Y. and Sobolev N. V. (2016) Low water contents in diamond mineral inclusions: Proto-genetic origin in a dry cratonic lithosphere. *Earth Planet. Sci. Lett.* **433**, 125–132.

Tomlinson E. L., Jones A. P. and Harris J. W. (2006) Co-existing fluid and silicate inclusions in mantle diamond. *Earth Planet. Sci. Lett.* **250**, 581–595.

Tumiati S., Tiraboschi C., Sverjensky D. A., Pettke T., Recchia S., Ulmer P., Miozzi F. and Poli S. (2017) Silicate dissolution boosts the CO 2 concentrations in subduction fluids. *Nat. Commun.* **8**(1), 1–11.

Vitale Brovarone A., Martinez I., Elmaleh A., Compagnoni R., Chaduteau C., Ferraris C. and Esteve I. (2017) Massive production of abiotic methane during subduction evidenced in metamorphosed ophicarbonates from the Italian Alps. *Nat. Commun.* **8**, 14134.

Walter M. J., Kohn S. C., Araujo D., Bulanova G. P., Smith C. B., Gaillou E., Wang J., Steele A. and Shirey S. B. (2011) Deep mantle cycling of oceanic crust: evidence from diamonds and their mineral inclusions. *Science* **334**, 54–57.

Wang H., van Hunen J. and Pearson D. G. (2015) The thinning of subcontinental lithosphere: The roles of plume impact and metasomatic weakening. *Geochem. Geophys. Geosyst.* **16**, 1156–1171.

Weiss Y., Class C., Goldstein S. L. and Hanyu T. (2016) Key new pieces of the HIMU puzzle from olivines and diamond inclusions. *Nature* **537**, 666–670.

Weiss Y., Griffin W., Bell D. and Navon O. (2011) High-Mg carbonatitic melts in diamonds, kimberlites and the sub-continental lithosphere. *Earth Planet. Sci. Lett.* **309**, 337–347.

Weiss Y., Griffin W. L. and Navon O. (2013) Diamond-forming fluids in fibrous diamonds: The trace-element perspective. *Earth Planet. Sci. Lett.* **376**, 110–125.

Weiss Y., Kessel R., Griffin W., Kiflawi I., Klein-BenDavid O., Bell D., Harris J. and Navon O. (2009) A new model for the evolution of diamond-forming fluids: Evidence from microin-clusion-bearing diamonds from Kankan, Guinea. *Lithos* **112**, 660–674.

Weiss Y., Kiflawi I., Davies N. and Navon O. (2014) High-density fluids and the growth of monocrystalline diamonds. *Geochim. Cosmochim. Acta* **141**, 145–159.

Weiss Y., McNeill J., Pearson D. G., Nowell G. M. and Ottley C. J. (2015) Highly saline fluids from a subducting slab as the source for fluid-rich diamonds. *Nature* **524**, 339–342.

Westerlund K. J., Shirey S. B., Richardson S. H., Carlson R. W., Gurney J. J. and Harris J. W. (2006) A subduction wedge origin for Paleoarchean peridotitic diamonds and harzburgites from the Panda kimberlite, Slave craton: evidence from Re–Os isotope systematics. *Contr. Mineral. Petrol.* **152**, 275–294.

Whitney D. L. and Evans B. W. (2010) Abbreviations for names of rock-forming minerals. *Am. Mineral.* **95**, 185–187.

Zhang C. and Duan Z. (2009) A model for C-O–H fluid in the Earth's mantle. *Geochim. Cosmochim. Acta* **73**, 2089–2102.

Associate editor: Horst R. Marschall